Newly imaged shape of the deep seismic zone within the subducting Pacific plate beneath the Hokkaido corner, Japan-Kurile arc-arc junction

Kei Katsumata, Naoto Wada,[1] and Minoru Kasahara
Institute of Seismology and Volcanology, Hokkaido University, Sapporo, Japan

Received 28 August 2002; revised 26 August 2003; accepted 15 September 2003; published 23 December 2003.

[1] The geometry of the deep seismic zone associated with the subducting Pacific plate beneath the North American plate in the Hokkaido corner, Japan-Kurile arc-arc junction has been investigated based on the hypocenters accurately relocated by a dense local seismographic network with three-dimensional *P* and *S* wave velocity structures. The model suggests that the lateral changes in the dip of the subduction zone are more rapid than previously believed. We found that the deep seismic zone in the Pacific plate dips at 20° to 30° on the side of the Japan arc, the dip angle increased in a narrow region around 143°–144°E by 10° to 20°, and the dip was 40° to 50° on the side of the Kurile arc. In the transitional zone around 143°–144°E an unusual distribution of microearthquakes has been discovered within the Pacific plate, which was located on a near-vertical plane with an area of 50 × 100 km^2 with strike that was perpendicular to the Kurile Trench axis. This feature was named the Tokachi-Oki slab-cracking zone. We suggest that this is a slab-cracking zone torn by the extensional stress due to the rapid lateral changes in the dip of the subduction zone. The slab-cracking zone may possibly grow into the large disruption or tear of the slab in the future. *INDEX TERMS:* 7218 Seismology: Lithosphere and upper mantle; 7230 Seismology: Seismicity and seismotectonics; 8150 Tectonophysics: Plate boundary—general (3040); *KEYWORDS:* carbon burial, sulfur, Paleogene

Citation: Katsumata, K., N. Wada, and M. Kasahara, Newly imaged shape of the deep seismic zone within the subducting Pacific plate beneath the Hokkaido corner, Japan-Kurile arc-arc junction, *J. Geophys. Res.*, *108*(B12), 2565, doi:10.1029/2002JB002175, 2003.

1. Introduction

[2] Little was known on the detailed shape of descending slabs at arc-arc junctions (Figure 1) where there can be abrupt changes in the trend of subduction zone forming corners. The shape of the subducting lithosphere is generally thought to follow the surface configuration of the trench and be continuous around the sharp bend. *Isacks and Molnar* [1971] suggested that in such a situation the slab would be either contorted or disrupted. The shape of the descending Pacific plate along the entire length of Japan and the Kurile Islands was evaluated based on mainly teleseismically determined seismicity compiled by the International Seismological Center [*Utsu*, 1974; *Burbach and Frohlich*, 1986; *Lundgren and Giardini*, 1990; *Chiu et al.*, 1991]. According to these previous studies the Pacific plate dips 30° beneath northern Honshu and 40° to 50° beneath the Kurile Islands. Both contortion and disruption of the Pacific plate was suggested at the Hokkaido corner, which is the junction of the Kurile and the Japan arcs [*Sasatani*, 1976; *Stauder and Mualchin*, 1976]. Although these previous studies provided preliminary images for the arc-arc junction, their spatial resolutions were relatively poor. For example, these studies could not detect the presently well-known double plane seismic zone under the northern coast of Honshu [*Hasegawa et al.*, 1978].

[3] *Hasegawa et al.* [1983] and *Suzuki et al.* [1983] mapped hypocenters determined by a local seismic network and presented a model for the geometry of the double seismic zone along the northern Honshu and the Hokkaido corner. They relocated hypocenters using simple one-dimensional (1-D) *P* and *S* wave velocity structures, which have limitations because strong lateral heterogeneities are expected to exist in the crust and the upper mantle of the Hokkaido corner region. In addition to the subducted Pacific plate, which is obviously one of the heterogeneities, the Kurile Islands arc is moving toward the southwest at a speed of 6–11 mm/year relative to the North American plate [*DeMets*, 1992] and has been colliding with the Japan arc since the middle Miocene, forming the arc-arc type Hidaka collision zone (HCZ) in and around the Hokkaido corner [e.g., *Kimura*, 1996]. Seismic reflection surveys suggested that the lower crust of the Kurile Islands arc was delaminated at the HCZ by the collision [*Tsumura et al.*, 1999]. The Hidaka Mountain Range (HMR) in the HCZ is being uplifted due to the collision. The heterogeneity related to the collision process should be taken into account when relocating hypocenters in this region.

[4] *Miyamachi et al.* [1994] applied an inverse method to *P* and *S* wave arrival time data observed at 52 seismographic

[1] Now at Shibetsu-cho Town Office, Shibetsu-cho, Japan.

0148-0227/03/2002JB002175$09.00

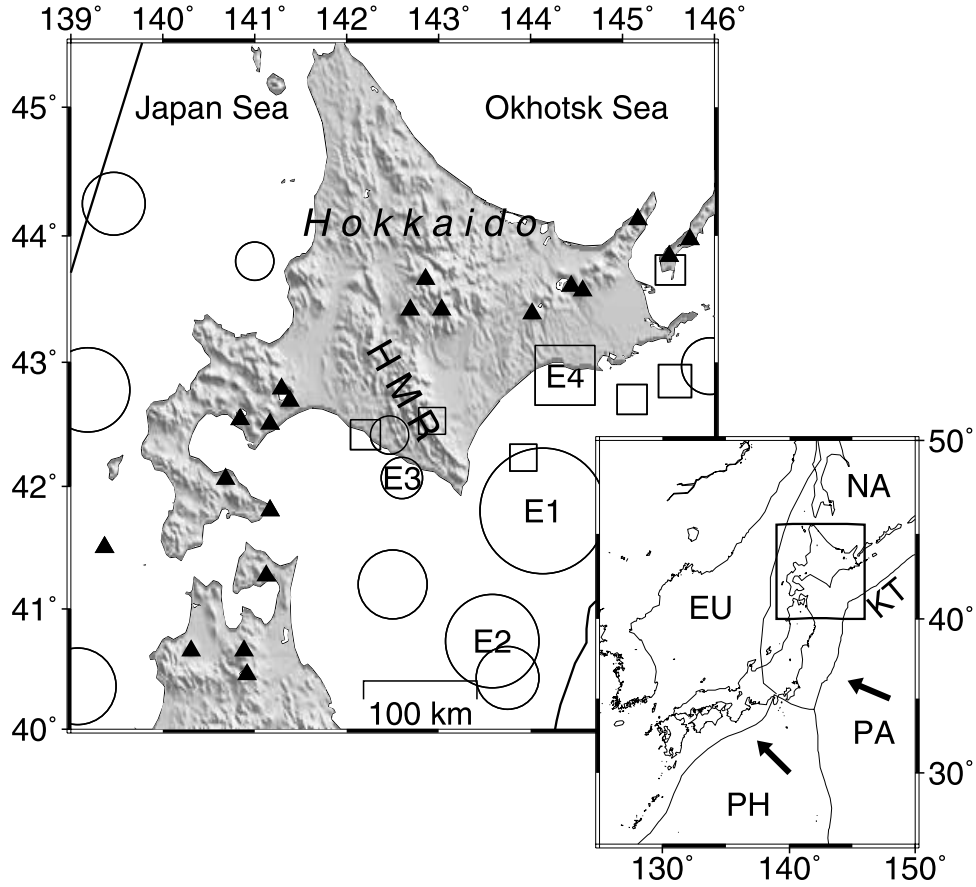

Figure 1. Hokkaido corner. Inset shows the study area and the plate configuration. The region in and around the Hidaka Mountain Range (HMR) is the Hidaka Collision Zone. Triangles are active volcanoes. Circles and rectangles indicate earthquakes with M = 7.0 or larger at depths shallower and deeper than 40 km, respectively, based on the catalog of the Japan Meteorological Agency from 1930. E1: Tokachi-Oki (M8.2) in 1952; E2: Tokachi-Oki (M7.9) in 1968; E3: Urakawa-Oki (M7.1) in 1982; and E4: Kushiro-Oki (M7.8) in 1993. PA, Pacific plate, PH, Philippine Sea plate; EU, Eurasian plate; NA, North American plate; and KT, Kurile Trench.

stations for 349 local earthquakes to determine simultaneously the three-dimensional (3-D) depth distributions of the Moho and the upper boundary of the Pacific plate along with 3-D P and S wave velocity distributions, station corrections and hypocenters.

[5] In this paper we used arrival time data observed by a new dense seismographic network and used the 3-D P and S wave velocity structures of *Katsumata et al.* [2002b] to relocate the hypocenters. On the basis of the relocated hypocenters we modeled the detailed geometry of the deep seismic zone of the subducting Pacific plate. We discovered some unusual distributions of the hypocenters, which were not detected by the previous studies. These results are presented and we discuss their implications for the tectonics around the Japan-Kurile arc-arc junction.

2. Tectonic Setting

[6] The Japan and Kurile arcs are two of the most active seismic regions of the Earth. *Hashimoto* [1984] reviewed the tectonic setting in and around the Japan-Kurile arc-arc junction in detail, so here we briefly summarize tectonics and seismicity, including new results from recent studies.

[7] The Pacific plate under the northwestern Pacific Ocean is descending beneath the Kurile Islands and Japan Islands, with the northern part of Honshu, Hokkaido and the Kurile Islands located on the North American or the Okhotsk plate [e.g., *Takahashi et al.*, 1999]. According to the NUVEL-1A model the Pacific plate around the Hokkaido corner moves in a N63°W direction at a speed of 83 mm/year relative to the North American plate [*DeMets et al.*, 1994].

[8] Great interplate earthquakes have occurred around the Hokkaido corner: the 1952 M = 8.2 Tokachi-Oki [*Kasahara*, 1976], the 1968 M = 7.9 Tokachi-Oki [*Kanamori*, 1971], the 1969 M = 7.8 Shikotan [*Abe*, 1973], and the 1958 M = 8.0 Etorofu [*Fukao and Furomoto*, 1979] earthquakes. Also, great earthquakes rupturing within the Pacific slab have occurred around the Hokkaido corner: the 1978 M = 7.7 Kunashiri Strait [*Kasahara and Sasatani*, 1985], the 1993 M = 7.8 Kushiro-Oki [*Ide and Takeo*, 1996; *Suzuki and Kasahara*, 1996; *Ozel and Moriya*, 1999], and the 1994 M = 8.2 Hokkaido-Toho-Oki [*Kikuchi and Kanamori*, 1995; *Katsumata et al.*, 1995; *Ozawa*, 1996] earthquakes. Great earthquakes rupturing within the oceanic lithosphere of subducting slab are relatively common events

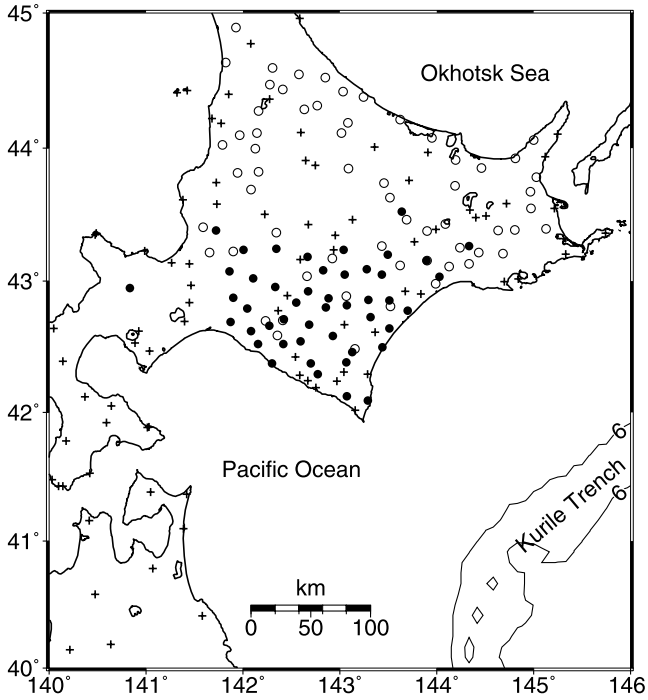

Figure 2. Seismographic stations used in this study. Solid circles, crosses, and open circles indicate the temporary stations operated from 1999 to 2001, permanent stations, and Hi-net stations, respectively.

in the world (e.g., the 1933 M_w = 8.4 Sanriku; the 1970 M_w = 7.9 Peru; the 1977 M_w = 8.2 Sumba Sea; and the 1994 M_w = 8.2 Bolivia). A noteworthy feature of the Hokkaido corner is that both types, interplate and lithospheric events, occur in the same region. *Suzuki and Kasahara* [1996] suggested that bending or unbending of the slab caused lithospheric-type great earthquakes in the Hokkaido corner.

3. Data

[9] We used waveform data from 47 seismographic stations temporally deployed in and around the HMR from July 1999 to July 2001 (Figure 2). Also, we used waveform data from the permanent seismic stations in Hokkaido and northern Honshu. These stations are maintained by the Institute of Seismology and Volcanology, Hokkaido University (ISV), the Japan Meteorological Agency, Tohoku University, Hirosaki University and the National Research Institute for Earth Science and Disaster Prevention (NIED). The high-sensitivity seismograph network (Hi-net) is constructed and maintained by NIED and began operation in Hokkaido in October 2000. We downloaded waveform data of earthquakes larger than M = 3.5 from the Web site of NIED during the period of the temporary observations. The data acquisition process was described in detail by *Katsumata et al.* [2002a].

4. Analyses

4.1. Relocation of Hypocenters

[10] Preliminary hypocenters were calculated by the program HYPOMH, which is based on a simple algorithm to find a maximum likelihood solution with the Bayesian approach [*Hirata and Matsu'ura*, 1987]. We assumed a 1-D P wave velocity structure: 5.8 km/s on the ground surface, 6.8 km/s, 7.6 km/s, and 9.0 km/s at depths of 30 km, 35 km and 405 km, respectively [*Suzuki et al.*, 1988]. The velocity structure is the same as that used for the hypocenter calculation in the ISV data processing system. The velocities at midpoint depths were calculated by linear interpolation. For instance we used a velocity of 6.3 km/s at 15 km for the midpoint between the ground surface and a depth of 30 km. The S wave velocity was given with the assumption that, $V_P/V_S = \sqrt{3}$ where V_p and V_s are P and S wave velocities, respectively. This assumption is equivalent to assuming that the Poisson's ratio is 0.25. The value of 0.25 applies mostly to crustal structures, while values in the mantle are typically higher (approximately 0.28) and so the V_P/V_S ratio is approximately 1.8. In general this ratio varies with changes in material composition.

[11] Since the crust and the upper mantle beneath the Hokkaido corner have very complicated geological structures [e.g., *Miyamachi et al.*, 1994; *Moriya et al.*, 1998], it is not appropriate to use a simple 1-D layered velocity structure for the hypocenter calculation. *Katsumata et al.* [2002b] determined 3-D P and S wave velocity structures in and around the Hokkaido corner by applying a tomographic method developed by *Zhao et al.* [1992] to arrival time data from shallow and intermediate-depth earthquakes. In the present study we assumed this 3-D velocity structures, and relocated approximately 4200 earthquakes using a method developed by *Zhao et al.* [1992]. All earthquakes we relocated had 10 or more P wave arrival time readings, and 5 or more S wave arrival time readings. Figure 3 shows the results of the relocation.

4.2. Horizontal and Vertical Shifts From 1-D to 3-D Structures

[12] We investigated the differences in the hypocenter determination using the 1-D and 3-D structures by measuring the spatial differences between the locations (Figure 4). In order to find a general pattern of hypocentral shift the study area was divided into blocks with sizes that were 0.25° in the horizontal direction and 15–50 km in the vertical direction. We calculated the averages of the horizontal and vertical shifts for blocks that included 10 or more earthquakes. We found that hypocenters moved by 3 to 5 km horizontally and 0 to 8 km vertically in all the layers. Although there were some exceptions, the horizontal shifts were usually outward from the center of the seismographic network and the depths became deeper. This pattern of the location shifts was probably caused by the high-velocity anomaly in the crust and the upper mantle beneath the HMR.

[13] The residual reduction in Figure 4 was defined for an earthquake as $(R_{1D} - R_{3D})/R_{1D}$, where R_{1D} and R_{3D} are the root mean square values of the P wave travel time residuals for the 1-D and 3-D velocity structures, respectively. We found that the reduction ranged from 10 to 30% in the study area. Especially in the HMR, we had a large reduction of 30% at almost all depths. This indicates that there are strong velocity heterogeneities beneath the mountain range; therefore the 1-D velocity structure is obviously

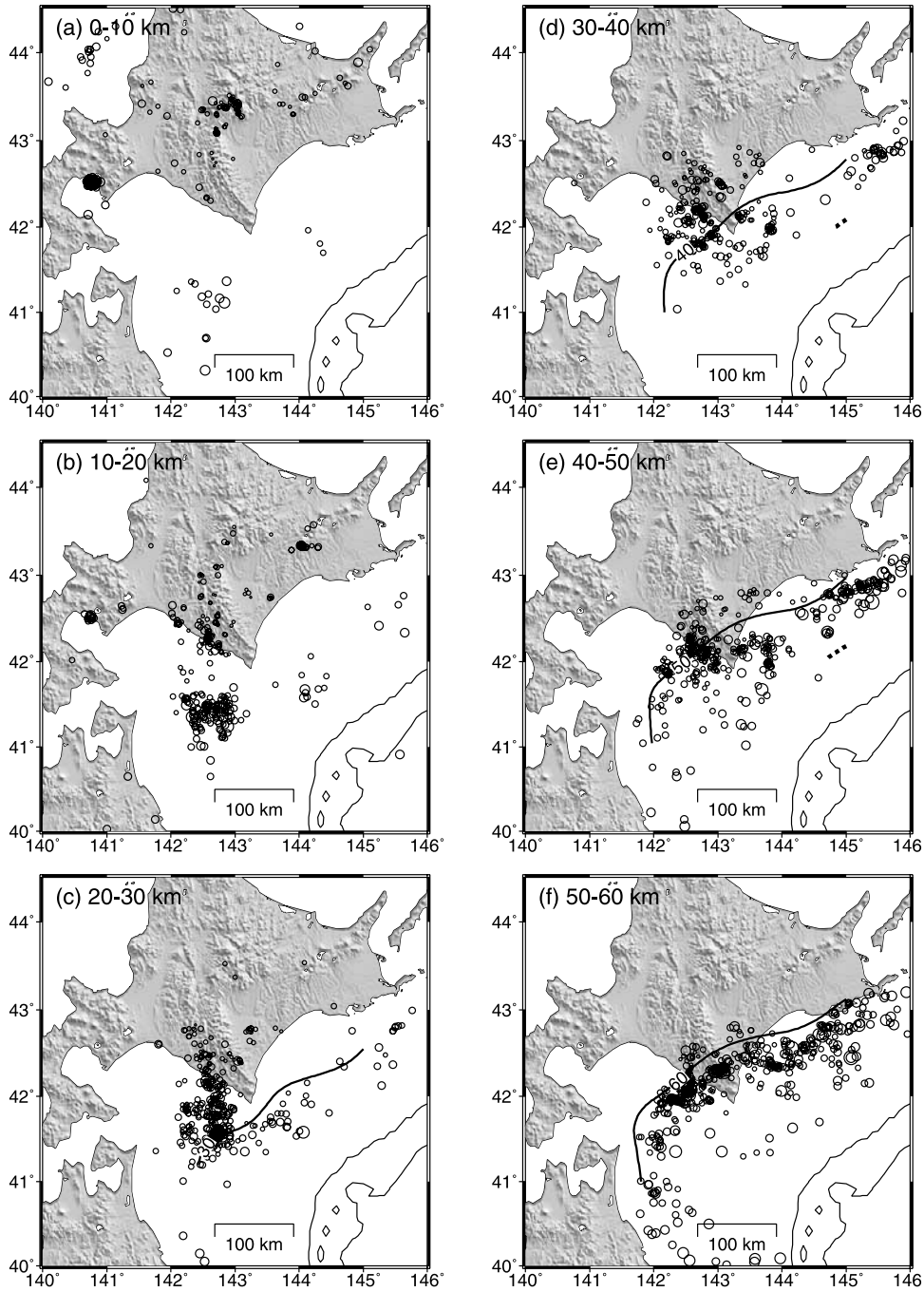

Figure 3. Epicentral distributions of the relocated earthquakes. The depth range is shown in the top left corner of each map. The solid and the broken lines denote the depths in kilometers to the upper and the lower surfaces, respectively, of the deep seismic zone modeled in the present study.

not appropriate for calculating hypocenters in and around this region.

4.3. Location Errors

[14] In order to estimate location errors we carried out a numerical simulation. For an earthquake location, we calculated model arrival times to the recording stations and added random noise to the travel times. Then we determined the hypocenter and examined the shift of hypocenter from the original location. This process was repeated one hundred times for each earthquake location and the location errors were estimated by how the resulting hypocenters were distributed. For the random noise, ±10% of the travel time was used. For instance if the travel time was 10.0 s at a station, the random values ranged from 9.0 to 11.0 s. A hypocenter calculated using the travel times with noise will be shifted from the one calculated using the travel times without the noise. We calculated the averages of the horizontal and vertical shifts for the one hundred hypocenters and defined these averages as the location error for

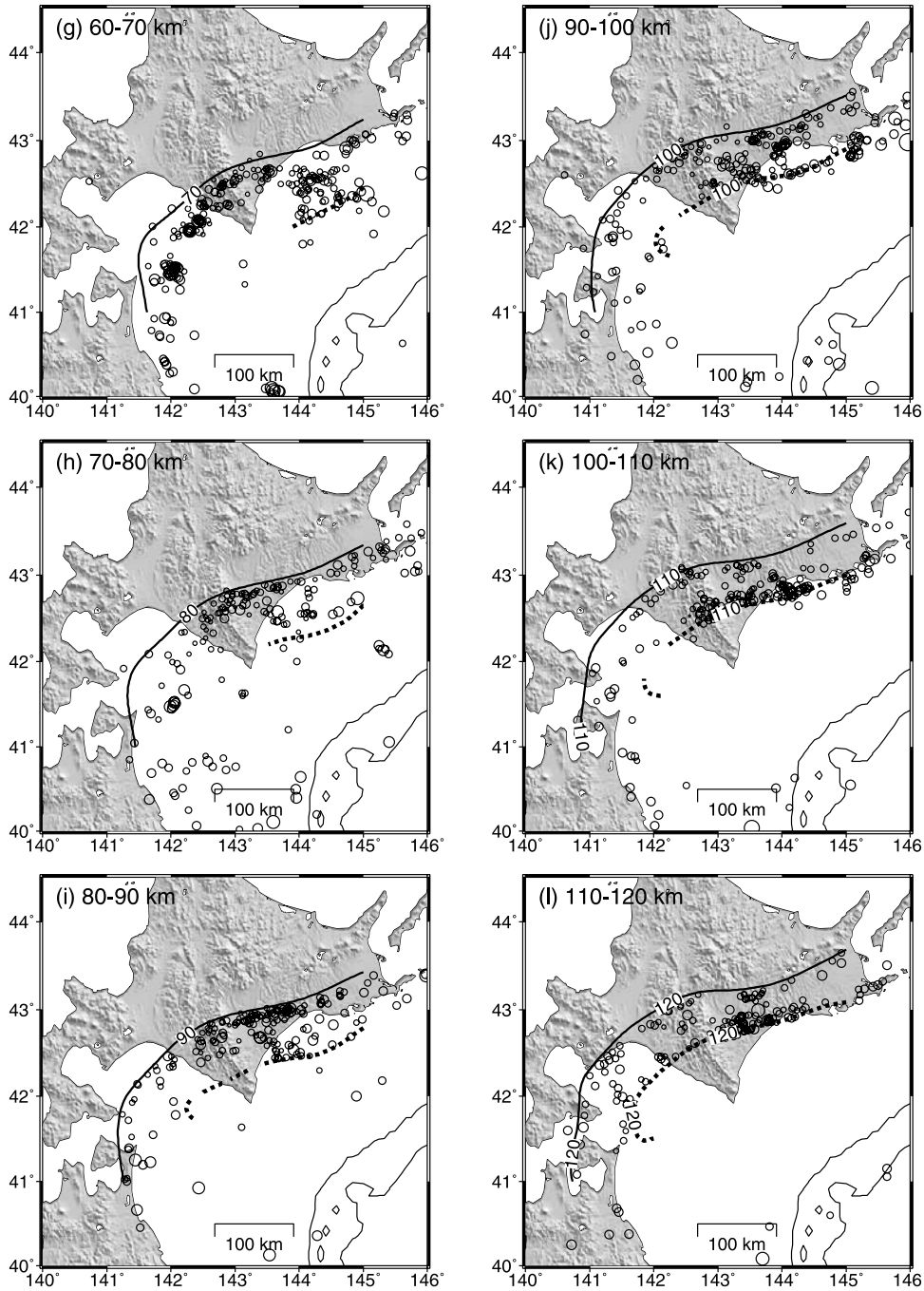

Figure 3. (continued)

the earthquake. The location error is mainly caused by an inappropriate assumption of velocity structures, reading errors depending on ground noise levels and poor station coverage. The method in this paper was very simple but we were able to simulate all three factors simultaneously. Moreover, the ±10% random noise we applied was a reasonable assumption since (1) the velocity perturbations obtained from the tomographic inversion were mostly smaller than ±10% in the study area [*Katsumata et al.*, 2002b] and (2) all reading errors were much smaller than ±10% of travel times.

[15] In order to find a general pattern of the hypocentral location error, the study area was divided into blocks 0.25° size in horizontal direction and 15–50 km in the vertical direction, and we calculated averages of the error for the blocks including 10 or more earthquakes. We found that the errors for the east-west and the north-south directions were 1 to 4 km in the crust at depths shallower than 30 km and increased as a function of depth (Figure 5). The errors for the vertical direction were 2 to 4 km in the land area and 6 to 10 km in the ocean area for depths shallower than 50 km. The vertical errors also increased as a function of depth.

[16] However, this uncertainty experiment could be a misleading test of the robustness of the earthquake locations, because all the noise in the simulation is uncorrelated.

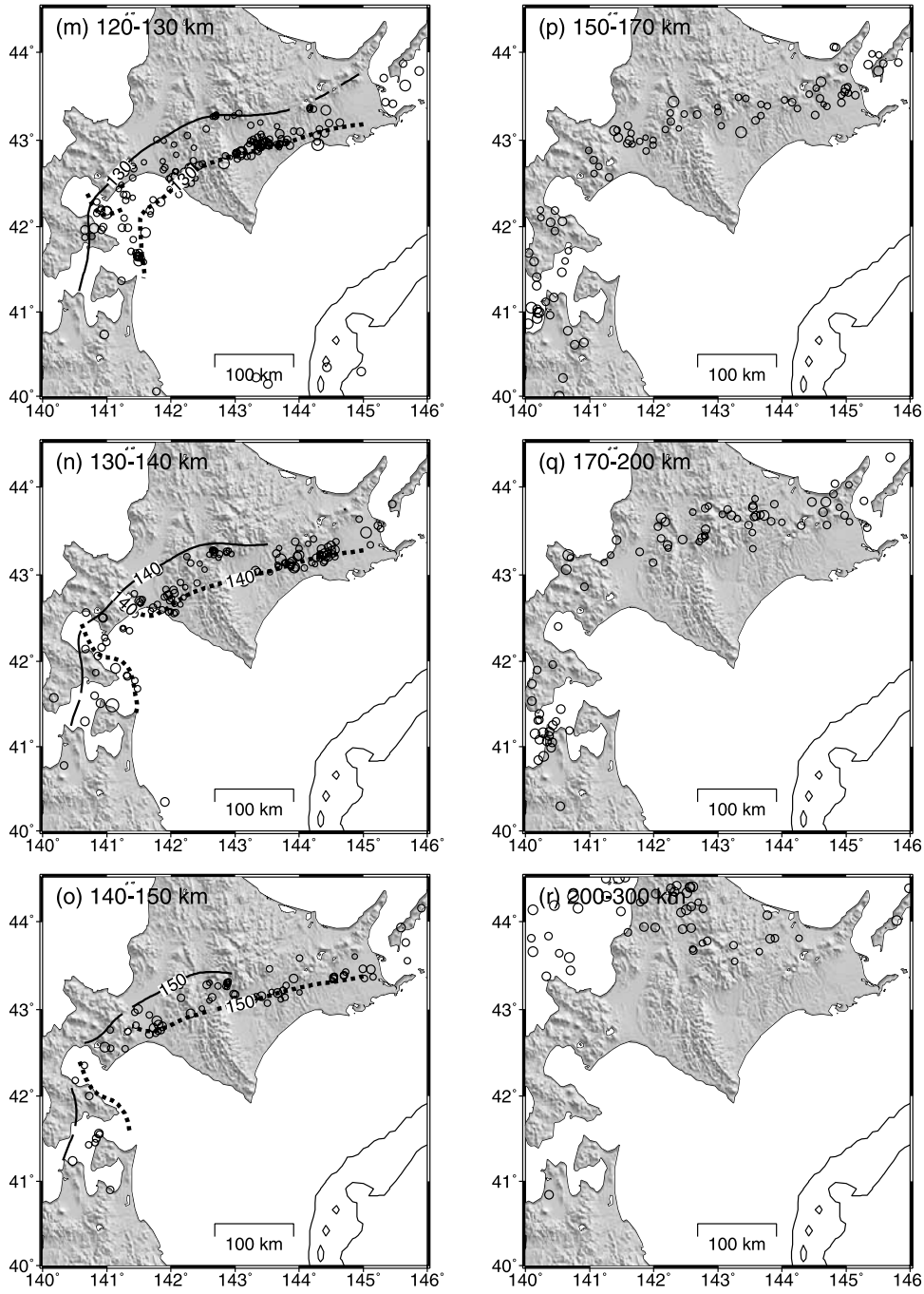

Figure 3. (continued)

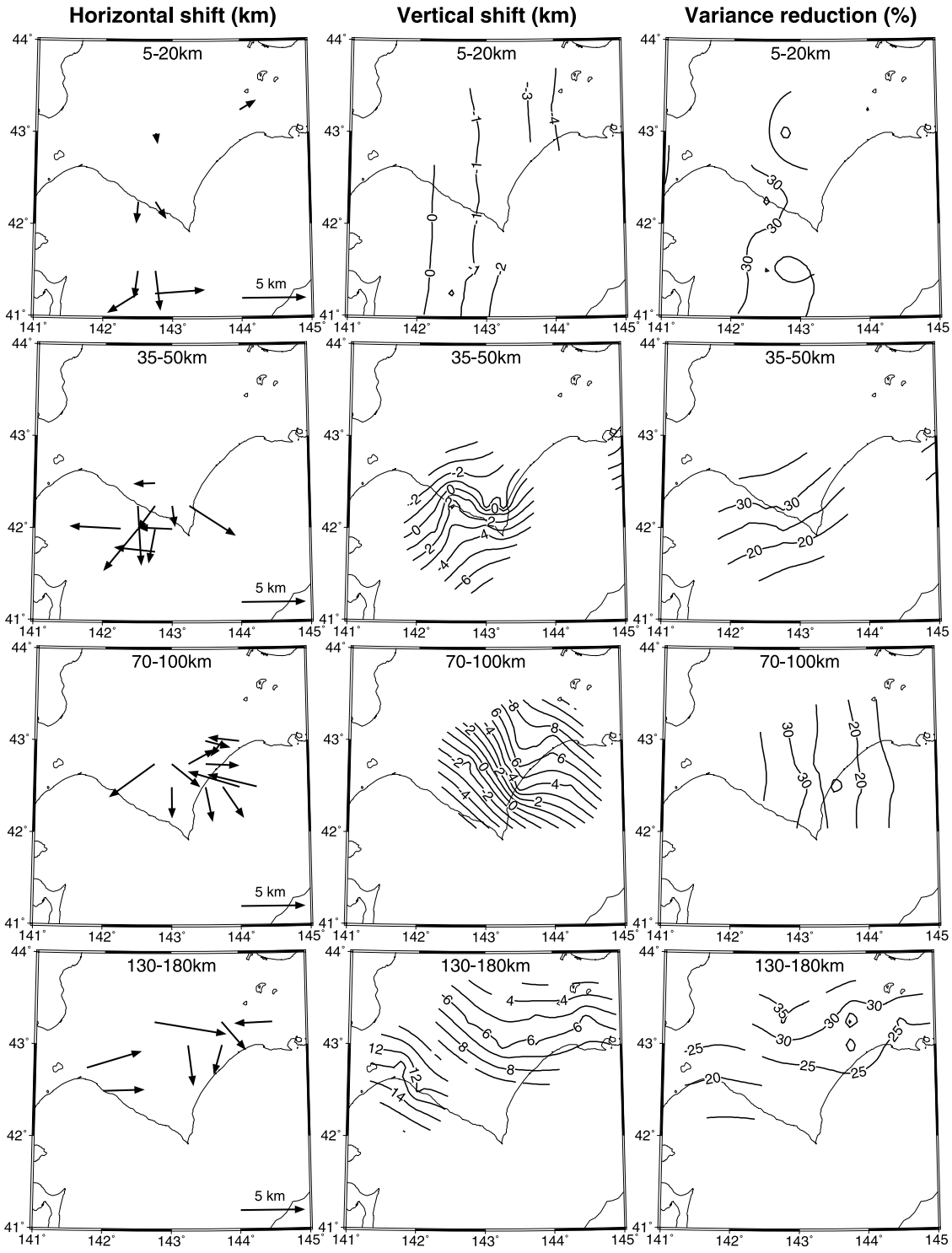

Figure 4. Horizontal and vertical shifts (km) and variance reductions (percentage) comparing the results for 1-D and 3-D velocity structures. The start and the end points of the arrows on the horizontal shift maps denote hypocenters determined using the 1-D and 3-D velocity structures, respectively. The hypocentral depth range is shown at the top of each map.

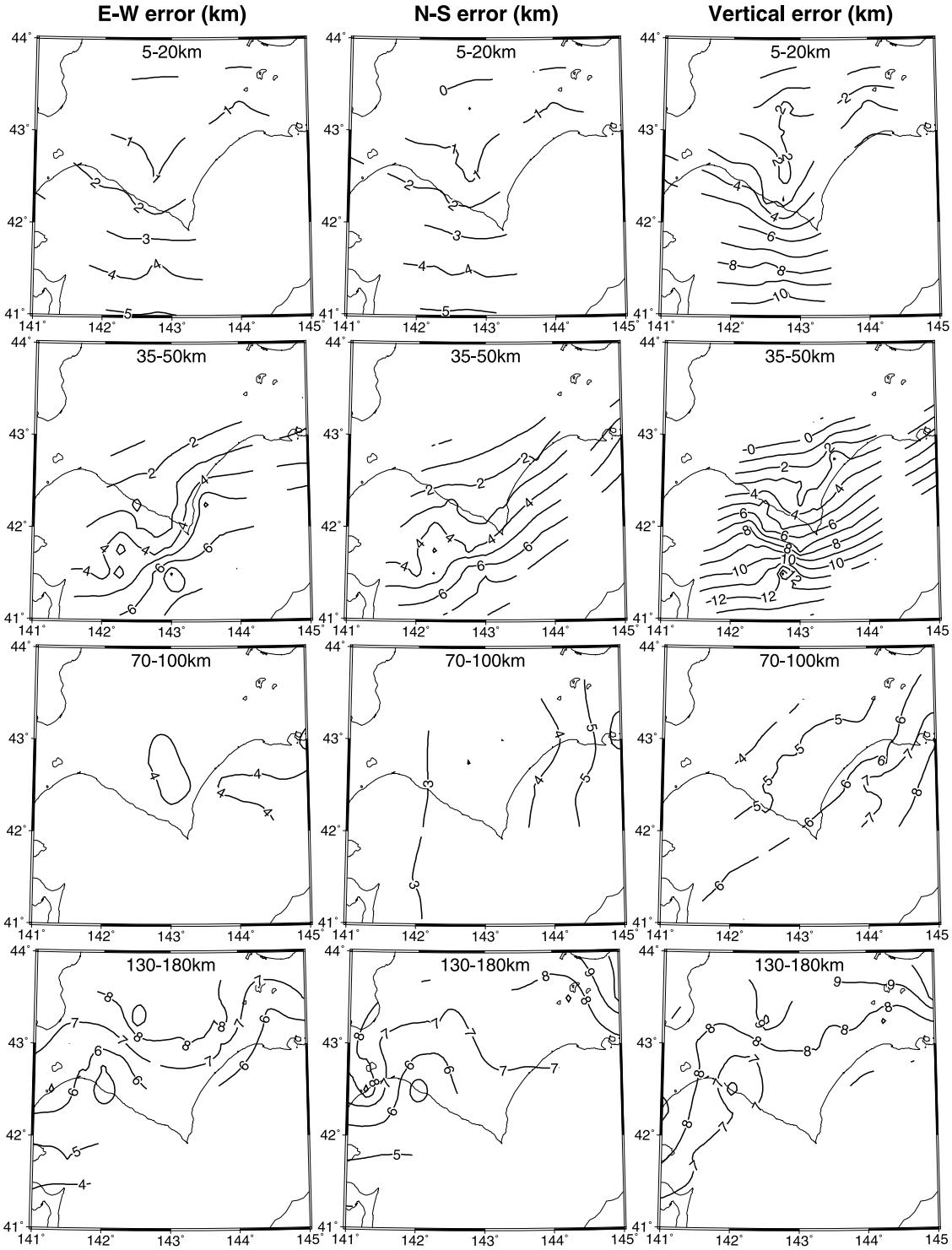

Figure 5. Location errors estimated by the numerical simulation. Contour lines are for 1 km intervals. The hypocentral depth range is shown at the top of each map.

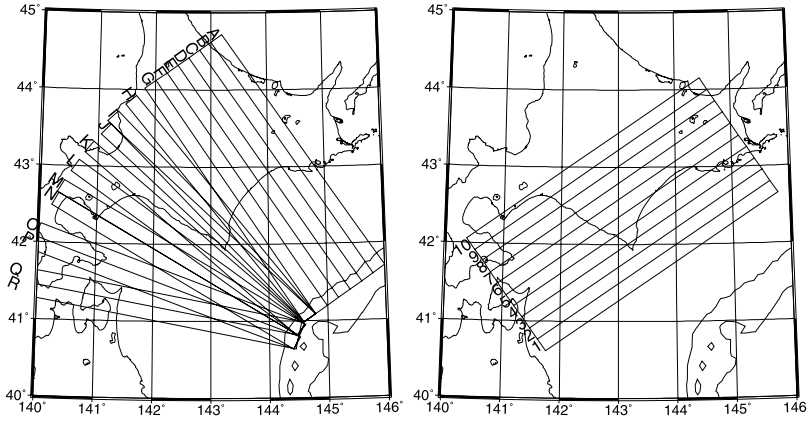

Figure 6. Locations and areas for the cross sections of the relocated earthquakes. Cross sections are aligned perpendicular and parallel to the Kurile Trench axis for A to R and for 1 to 10, respectively.

There is a potential problem of correlated errors due to some unmodeled seismic structure. We claim that random noise may mimic the effects of missing velocity structure, reading errors and poor station coverage, but only reading errors could plausibly be assumed to cause uncorrelated errors in travel time data.

4.4. Modeling the Shape of the Deep Seismic Zone

[17] To model the shape of the deep seismic zone in the Pacific plate we selected 3616 earthquakes with $M = 2.0$ or larger among the relocated hypocenters. We made vertical cross sections of earthquakes along directions shown in Figure 6, which have widths of 20 km perpendicular and parallel to the Kurile Trench axis. We found that the deep seismic zone is not clearly divided into two planes in some regions of the Hokkaido corner. In these regions, earthquakes occur not only on the two seismic planes but also in between and we were not able to identify the location of the two planes. Therefore we defined the upper and the lower surfaces of the deep seismic zone, as shown in Figure 7. The deep seismic zone is enveloped by these surfaces on the top and the bottom. Note that we used the term ''surface'' rather than ''plane'' in the present study. Hereafter the term of ''the double seismic plane'' is used to describe seismicity that is clearly divided into two separate seismic planes. In order to fit a surface to the seismicity, we measured on the cross sections the depths to the upper and the lower surfaces at grid points spaced at 0.2° in latitude and longitude. The number of the measured points was 228 and 112 for the upper and the lower surfaces, respectively (see Table 1). Except for profiles K, L and M, the deep seismic zone was identified easily because seismicity in the crust and the mantle wedge did not overlap with the deep seismic zone. For the profiles K, L and M the depth to the upper surface was determined by interpolation between the deep and the shallow portions with the assumption that the deep seismic zone is more or less smooth and continuous.

[18] We represent the two surfaces by linear splines interpolating a grid of 9 × 8 nodes, spaced 1° in longitude and 0.5° in latitude. Figures 8 and 9 show the upper and the lower surfaces, respectively, overlaid on the seismicity. We found that the surfaces modeled by linear splines represent well the upper and the lower boundaries of seismicity of the deep seismic zone.

5. Results

5.1. Rapid Lateral Change in Subduction Angle

[19] We constructed a depth distribution model to the upper and the lower surfaces of the deep seismic zone in the Pacific plate (Figure 10). The most outstanding feature is that the upper surface significantly changed in dip angle. The dip angles are 20° to 30° in the western part of the study area which belongs to the Japan arc, and 40° to 50° in the eastern part which belong to the Kurile Islands arc. The rapid change in dip angle of 10° to 20° takes place between 143°E and 144°E. The superposition of the upper surfaces for profiles A to M shows this rapid change more clearly (Figure 11). The slope is similar and gentle, 20° to 30°, for profiles M to K. Between profiles K and C it is obvious that the dip angle changes rapidly. The slope is similar and steep,

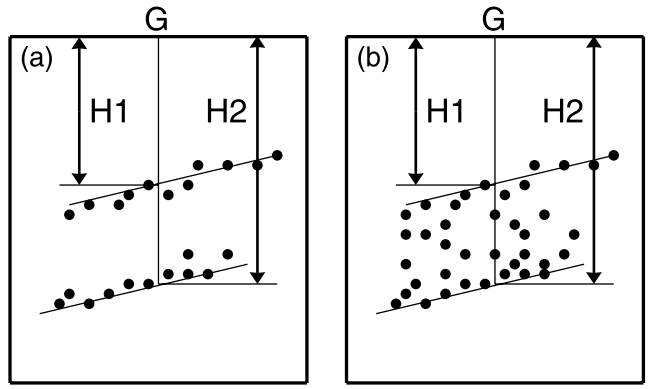

Figure 7. Definition used to determine the upper and the lower surfaces of the deep seismic zone. These figures schematically illustrate vertical cross sections perpendicular to the trench axis. (a) Seismicity clearly appearing on double plane structure. (b) Seismicity not clearly divided into the two planes. G is a grid point where we measure the depths to the surfaces H1 and H2, which correspond to the depths to the upper and the lower surfaces, respectively.

Table 1. Depths to the Upper and Lower Surfaces of the Deep Seismic Zone

Longitude, °E	Latitude, °N	Upper Surface, km	Lower Surface, km
140.0	41.2	178.4	···
140.2	41.2	161.6	···
140.2	41.4	157.0	···
140.2	41.8	189.0	···
140.4	41.2	146.3	···
140.4	41.4	146.3	···
140.4	41.8	170.7	···
140.6	41.2	129.6	···
140.6	41.4	132.6	···
140.6	41.8	152.4	···
140.6	42.0	129.6	···
140.6	42.2	138.7	167.7
140.8	41.2	109.8	···
140.8	41.4	112.8	···
140.8	41.6	118.9	···
140.8	41.8	112.8	···
140.8	42.0	122.0	157.0
140.8	42.2	128.0	···
140.8	42.6	143.3	···
141.0	41.4	100.6	···
141.0	41.6	106.7	···
141.0	41.8	102.1	···
141.0	42.0	111.3	···
141.0	42.2	114.3	···
141.0	42.4	126.5	···
141.0	42.6	152.4	···
141.0	42.8	143.3	···
141.2	41.2	91.5	···
141.2	41.4	91.5	···
141.2	41.6	94.5	···
141.2	41.8	89.9	···
141.2	42.0	99.1	143.3
141.2	42.2	100.6	···
141.2	42.4	114.3	···
141.2	42.6	135.7	···
141.2	42.8	132.6	···
141.2	43.2	170.7	···
141.4	41.2	76.2	···
141.4	41.4	79.3	···
141.4	41.6	80.8	···
141.4	41.8	77.7	143.3
141.4	42.0	85.4	140.2
141.4	42.2	97.6	···
141.4	42.4	100.6	···
141.4	42.6	118.9	140.2
141.4	42.8	126.5	···
141.4	43.2	175.3	···
141.4	43.4	175.3	···
141.6	41.2	68.6	···
141.6	41.4	70.1	···
141.6	41.6	62.5	126.5
141.6	41.8	70.1	123.5
141.6	42.0	75.6	118.9
141.6	42.2	86.9	132.6
141.6	42.4	91.5	···
141.6	42.6	108.2	138.7
141.6	42.8	128.0	154.0
141.6	43.0	137.2	164.6
141.6	43.2	149.4	···
141.8	41.2	57.9	···
141.8	41.4	57.9	···
141.8	41.6	50.3	115.9
141.8	41.8	61.0	···
141.8	42.0	61.0	···
141.8	42.2	79.3	123.5
141.8	42.4	96.0	···
141.8	42.6	99.1	141.8
141.8	42.8	114.3	152.4
141.8	43.0	128.0	···
142.0	41.4	42.7	···
142.0	41.4	45.7	···
142.0	41.6	45.7	···
142.0	41.8	51.8	···
142.0	42.0	59.5	···
142.0	42.2	73.2	···
142.0	42.4	83.8	128.0
142.0	42.6	91.5	138.7
142.0	42.8	100.6	149.4
142.0	43.0	118.9	160.1
142.0	43.2	149.4	182.9
142.2	41.2	33.5	···
142.2	41.4	36.6	···
142.2	41.6	42.7	···
142.2	41.8	45.7	93.0
142.2	42.0	59.5	···
142.2	42.2	64.0	···
142.2	42.4	76.2	126.5
142.2	42.6	85.4	134.1
142.2	42.8	99.1	143.3
142.2	43.0	115.9	160.1
142.2	43.4	155.5	···
142.4	41.4	36.6	···
142.4	41.6	39.6	···
142.4	41.8	39.6	···
142.4	42.0	59.5	···
142.4	42.2	57.9	···
142.4	42.4	62.5	118.9
142.4	42.6	82.3	125.0
142.4	42.8	93.0	138.7
142.4	43.0	102.1	···
142.4	43.2	126.5	···
142.4	43.4	149.4	···
142.6	41.4	32.0	···
142.6	41.6	36.6	···
142.6	41.8	36.6	···
142.6	42.0	54.9	···
142.6	42.2	48.8	102.1
142.6	42.4	61.0	109.8
142.6	42.6	77.7	120.4
142.6	42.8	83.8	···
142.6	43.0	99.1	···
142.6	43.2	123.5	···
142.6	43.4	140.2	189.0
142.8	41.4	29.0	···
142.8	41.6	32.0	···
142.8	41.8	39.6	···
142.8	42.0	41.2	···
142.8	42.2	54.9	···
142.8	42.4	57.9	99.1
142.8	42.6	68.6	115.9
142.8	42.8	79.3	131.1
142.8	43.0	96.0	···
142.8	43.2	120.4	169.2
142.8	43.4	149.4	182.9
141.4	41.6	···	195.1
143.0	41.2	22.9	···
143.0	41.4	25.3	···
143.0	41.6	29.0	···
143.0	41.8	39.6	···
143.0	42.0	37.2	···
143.0	42.2	45.7	···
143.0	42.4	51.8	100.6
143.0	42.6	62.5	111.3
143.0	42.8	73.2	129.6
143.0	43.0	100.6	149.4
143.0	43.2	120.4	163.1
143.2	41.4	24.4	···
143.2	41.6	25.9	···
143.2	41.8	31.4	···
143.2	42.0	39.6	···
143.2	42.2	42.7	···
143.2	42.4	45.7	···
143.2	42.6	61.0	109.8
143.2	42.8	76.2	128.0
143.2	43.0	93.0	138.7

Table 1. (continued)

Longitude, °E	Latitude, °N	Upper Surface, km	Lower Surface, km
143.2	43.2	112.8	157.0
143.4	41.4	21.3	···
143.4	41.8	30.5	···
143.4	42.0	33.5	···
143.4	42.2	38.1	···
143.4	42.4	48.8	···
143.4	42.6	51.8	106.7
143.4	42.8	71.6	122.0
143.4	43.0	88.4	132.6
143.4	43.2	109.8	155.5
141.6	42.2	···	201.2
143.6	41.4	18.3	···
143.6	41.6	21.3	···
143.6	41.8	26.5	···
143.6	42.0	29.0	···
143.6	42.2	35.1	···
143.6	42.4	41.2	86.9
143.6	42.6	54.9	105.2
143.6	42.8	68.6	117.4
143.6	43.0	83.8	137.2
143.6	43.2	112.8	155.5
141.8	41.2	···	175.3
141.8	41.4	···	182.9
143.8	41.6	19.8	···
143.8	41.8	22.0	···
143.8	42.0	22.9	···
143.8	42.2	32.0	74.7
143.8	42.4	42.7	91.5
143.8	42.6	50.3	102.1
143.8	42.8	64.0	115.9
143.8	43.0	82.3	132.6
143.8	43.2	103.7	150.9
141.8	42.8	···	164.6
144.0	41.6	17.4	···
144.0	41.8	19.8	···
144.0	42.0	22.9	···
144.0	42.2	29.0	77.7
144.0	42.4	48.8	91.5
144.0	42.6	48.8	100.6
144.0	42.8	68.6	114.3
144.0	43.0	79.3	131.1
144.0	43.2	105.2	144.8
144.2	41.6	12.2	···
144.2	41.8	16.8	···
144.2	42.0	15.2	65.5
144.2	42.2	35.1	···
144.2	42.4	35.1	82.3
144.2	42.6	51.8	102.1
144.2	42.8	62.5	112.8
144.2	43.0	74.7	126.5
144.2	43.2	96.0	140.2
142.2	41.2	···	167.7
142.2	41.4	···	70.1
144.4	42.6	45.7	94.5
144.4	42.8	59.5	108.2
144.4	43.0	70.1	125.0
144.4	43.2	88.4	140.2
144.4	43.4	112.8	157.0
144.6	42.4	29.0	73.2
144.6	42.6	45.7	93.0
144.6	42.8	48.8	105.2
144.6	43.0	67.1	···
144.6	43.2	76.2	134.1
142.4	41.4	···	161.6
144.8	42.2	18.3	59.5
144.8	42.4	27.4	···
144.8	42.6	42.7	88.4
144.8	42.8	41.2	89.9
144.8	43.0	57.9	109.8
144.8	43.2	68.6	···
144.8	43.4	97.6	···
144.8	43.6	118.9	181.4
142.4	42.6	···	208.8

Table 1. (continued)

Longitude, °E	Latitude, °N	Upper Surface, km	Lower Surface, km
144.8	44.0	160.1	···
142.4	42.8	···	70.1
145.0	42.6	36.6	71.6
145.0	42.8	41.2	···
145.0	43.0	47.3	109.8
145.0	43.2	67.1	···
145.0	43.4	93.0	155.5
145.0	43.6	105.2	175.3
145.2	42.2	18.3	···
145.2	42.4	19.8	53.4
145.2	42.6	24.4	···
145.2	42.8	36.6	97.6
145.2	43.0	42.7	100.6
145.2	43.2	65.5	126.5
145.2	43.4	77.7	146.3
142.6	42.6	···	143.3
145.4	42.4	13.7	···
145.4	42.8	29.0	···
145.4	43.0	39.0	99.1
145.4	43.2	50.3	115.9
145.4	43.4	79.3	125.0

40° to 50°, for profiles C to A. We suggest that profiles M to K are representative of the dip of the deep seismic zone in the Japan arc and profiles C to A are representative of the dip of the Kurile Island arc. There is a probably a transitional zone between profiles K and C. Taking into account the hypocenter determination error as discussed in the section 4.3, the uncertainty of the depths in Figures 10 and 11 is up to ±5 km. Although this uncertainty is not small, the final conclusions on the shape or the dip of the seismic zone are not greatly affected by the location errors in the present study.

[20] Moreover seismicity on the upper and lower surfaces showed an anomaly around the transitional zone. Few earthquakes shallower than 100 km occurred around the lower surface west of about 144°E (see Figures 3g, 3h, 8g, 8h, and 8i). Few earthquakes deeper than 120 km occurred around the upper surface east of about 144°E as pointed out by *Hasegawa et al.* [1983] (see Figures 8c and 8d). Except for these regions the seismicity was active around both the upper and the lower surfaces. The boundary between active and non-active regions was very sharp and corresponded well to the zone where the dip angle of the upper surface changes rapidly.

5.2. Unusual Earthquake Cluster Within the Pacific Plate

[21] We found that many earthquakes occurred on a near vertical plane within the Pacific plate around the transitional zone where the dip angle of the upper surface changed rapidly (Figure 12). In this region, the upper and the lower seismic planes exist rather clearly in the Pacific plate at the depths of 50 and 100 km, respectively, and the earthquake cluster was located between the two seismic planes, where usually few earthquakes occur in the typical double seismic zone of northern Honshu. The dip of this plane was 80° toward the east and the strike was perpendicular to the Kurile Trench axis. The area of the near-vertical plane was 50 km in the dip direction × 100 km in the strike direction. As mentioned above the deep seismic zone within the Pacific plate changes subduction angle by 10° to 20° and

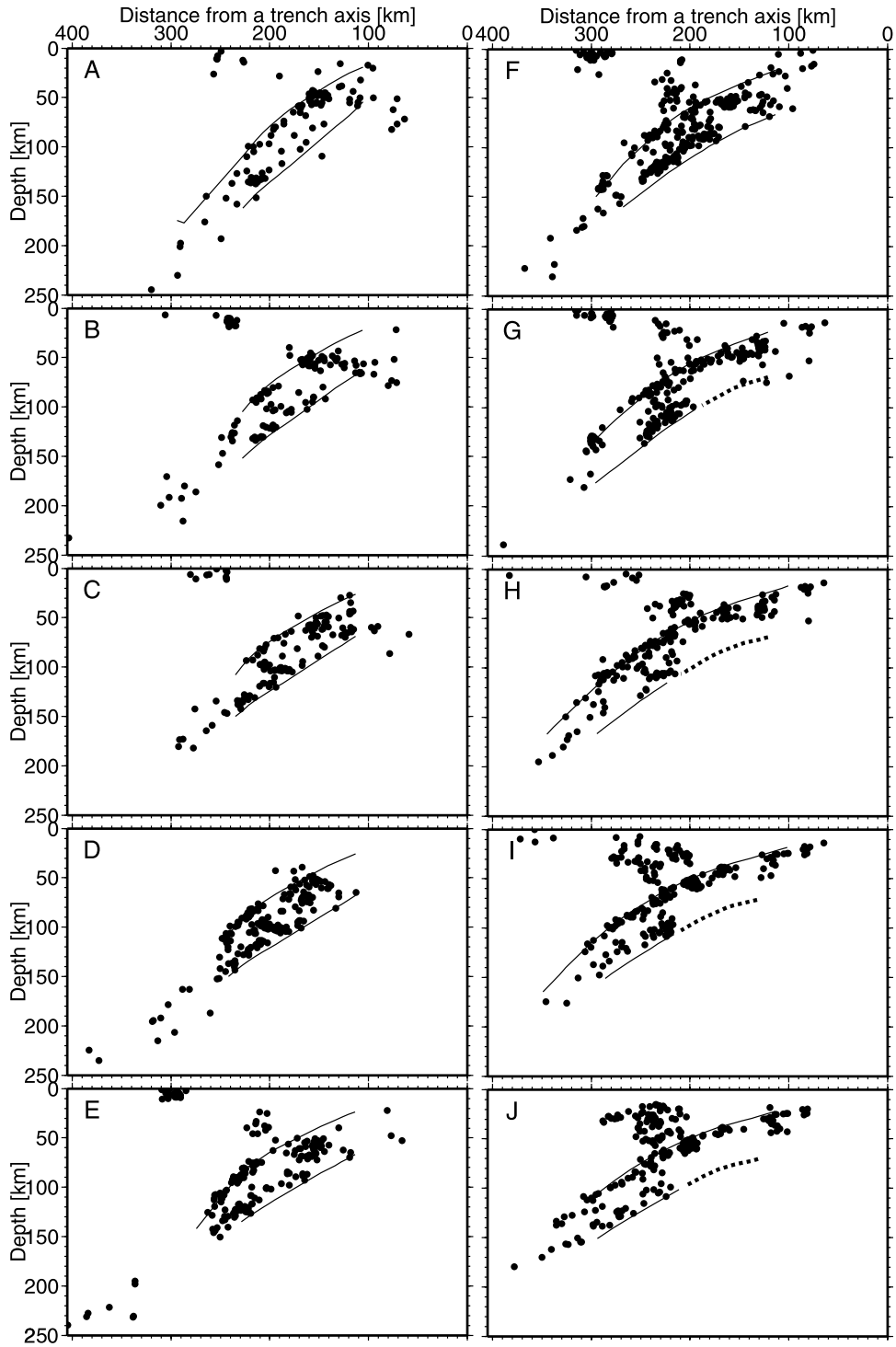

Figure 8. Cross sections perpendicular to the Kurile Trench axis (a–r) as shown on Figure 6. The solid lines denote the upper and the lower surfaces of the deep seismic zone. The dashed lines indicate the low seismicity area around the lower surface.

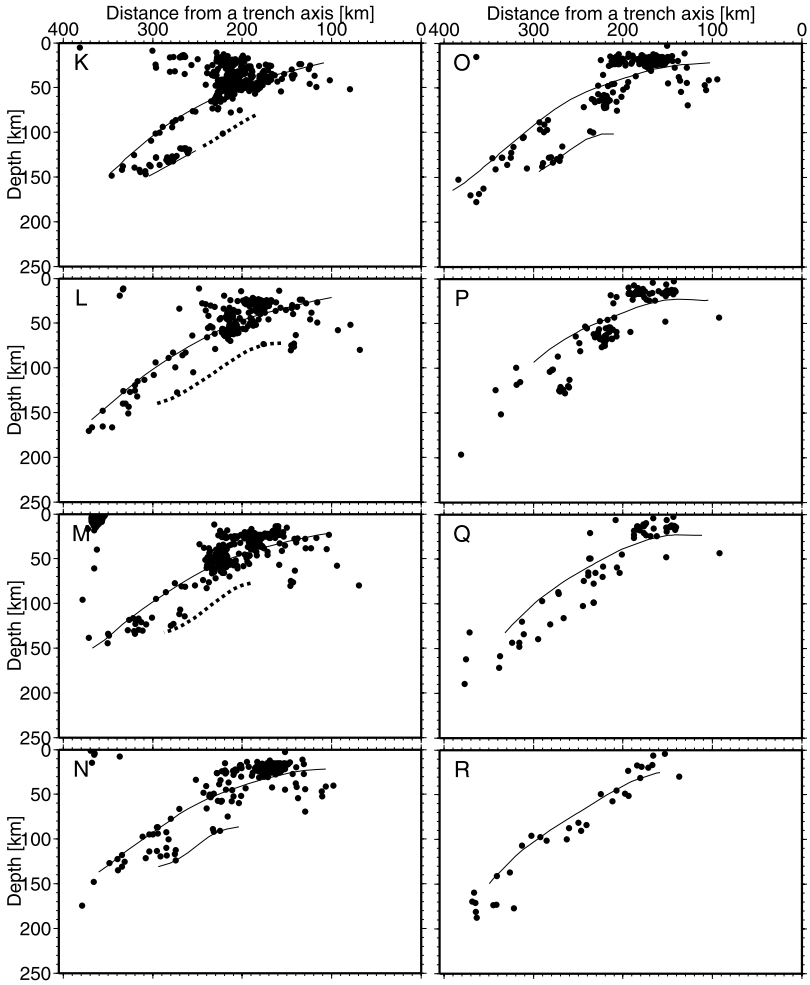

Figure 8. (continued)

the seismic activity showed the anomalies around this near-vertical earthquake cluster.

[22] Moreover, unusual earthquakes occurred in the mantle shallower than the upper surface of the deep seismic zone and deeper than the Moho. The depth to the Moho ranges from 30 to 40 km in this region [*Miyamachi et al.*, 1994]. Seismicity at distances of 0 to 50 km on Figure 12b is located in the HCZ and is related to the collision between the Japan arc and the Kurile Islands arc [e.g., *Moriya et al.*, 1998]. We found another cluster of seismicity in the mantle wedge at distances from 60 to 90 km on Figure 12c. This is more obvious on the map views in Figures 3e and 3f around (42.8°N, 143.3°E). We checked carefully the arrival time data of these earthquakes and we found no erroneous readings. No previous studies have reported this seismicity, which might be also related to the collision process.

6. Discussions

[23] Using arrival time data from a new dense seismographic network we assumed 3-D *P* and *S* wave velocity structures and relocated hypocenters of microearthquakes. On the basis of the relocated hypocenters we constructed a model of the 3-D shape of the deep seismic zone in the Pacific plate in and around the Hokkaido corner, Japan. The model suggests that lateral change in subduction angle is more rapid than previously believed.

6.1. Comparison With Previous Studies

[24] *Miyamachi et al.* [1994] obtained the shape of the upper boundary of the Pacific plate in and around the Hokkaido corner based on a 3-D *P* wave velocity inversion. They did not determine the depths to the deep seismic zone but instead the depths of velocity boundaries, such as the Moho and the upper surface of the Pacific plate. Since they found that earthquakes occurring in the upper seismic plane of the deep seismic zone were located on or just beneath the upper surface of the Pacific plate, we were able to compare their results with ours. Although our model is consistent for the most part with the Miyamachi model regarding the shape of the upper boundary of the Pacific plate (Figures 13a and 13b), the upper surface of the deep seismic zone in our model dips more steeply than that of the Miyamachi model (Figure 14b). The contours for depths of 80 km are in good agreement with each other. Since the contours of the Miyamachi model were not parallel to the Kurile Trench axis in the eastern part of the study area, our model is more reasonable than the Miyamachi model.

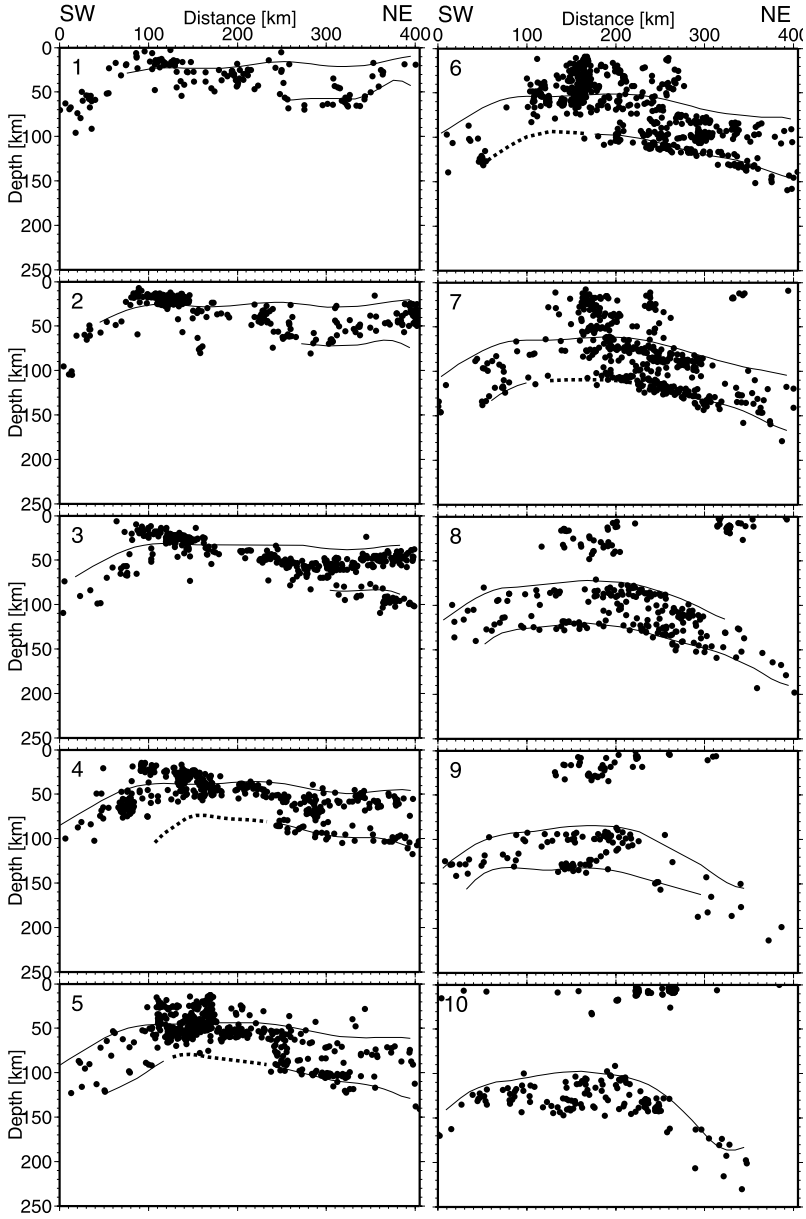

Figure 9. Cross sections parallel to the Kurile Trench axis. The solid lines denote the upper and the lower surfaces of the deep seismic zone. The dashed lines indicate the low seismicity area around the lower surface.

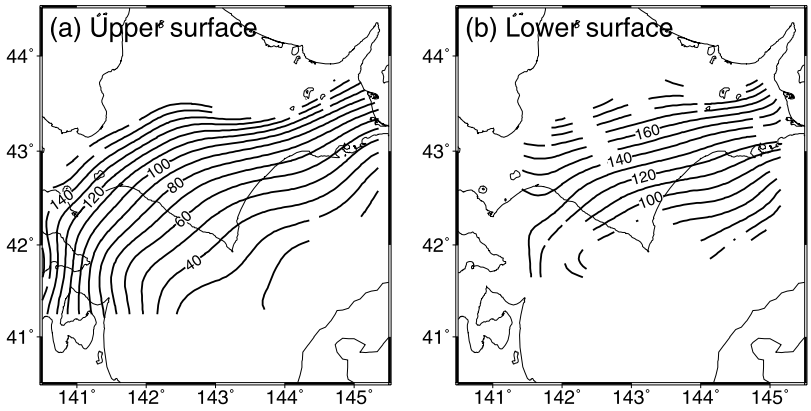

Figure 10. A model of the shape of the deep seismic zone: (a) depths to the upper surface and (b) depths to the lower surface. Contour interval is 10 km.

[25] *Hasegawa et al.* [1983] presented a model for the shape of the double seismic zone beneath northern Honshu and the Hokkaido corner. The upper seismic plane of the double seismic zone in their model is 10 to 20 km deeper than that of our model at the Hokkaido corner (Figures 13c and 13d). This is probably caused by not using an appropriate 3-D velocity structure when relocating earthquakes. Moreover the seismic plane of their model shows little change in dip (Figure 14a). The dips are ~30° for both northern Honshu and the Hokkaido corner.

6.2. Slab-Cracking Zone Within the Pacific Plate: Initial Stage of Slab Tearing

[26] *Moriya* [1978] suggested a folded structure of the Pacific plate for the same region where we found the unusual earthquake cluster within the Pacific plate, although his interpretation was based on poorly located hypocenters, since there were only a small number of seismographic stations at that time. This was the first report on the unusual distribution of earthquakes in the deep seismic zone beneath the Hokkaido corner.

[27] In order to examine the state of stress around the transition zone, we plotted focal mechanisms of earthquakes that occurred on the upper surface of the deep seismic zone. *Katsumata et al.* [2002a] determined 351 focal mechanisms in the Hokkaido corner region for the period between August 1999 and August 2001 by using polarities of *P* wave first motions. We selected 33 events with magnitude 3.0 or larger among the 351 focal mechanisms on the upper surface of the deep seismic zone and relocated the hypocenters using the 3-D velocity structure described in section 4.1 (Figures 15 and 16 and Table 2). The nodal planes for these earthquakes were constrained very well. We found that the 33 focal mechanisms, except for the earthquake number 5, were classified into five different types: (1) type 1 (the focal mechanism beach balls are black in Figure 15) represented by earthquake numbers 1, 2, 4, 6, 7, 8, 9, 10, 11, 12, 14, and 15; (2) type 2 (red) represented by earthquake numbers 18, 19, 20, 23, 24, 27, and 28; (3) type 3 (green) represented by earthquake numbers 21, 22, 25, 26, 30, and 31; (4) type 4 (yellow) represented by earthquake numbers 3, 13, 16, and 17; and (5) type 5 (blue) represented by earthquake numbers 29, 32, and 33. Focal mechanisms of type 1 and type 5 are low-angle-thrusts, which is consistent with *Kosuga et al.* [1996]. Three centroid moment tensor solutions determined by Harvard University which are low-angle thrust events in the region close to the trench axis are also plotted on Figure 15. Earthquakes in types 2 and 3 are located in the transitional zone. The focal mechanisms are normal faults or strike-slip faults. Tensional axes are in the ENE-WSW direction for type 2 and in the N-S or NNW-SSE direction for type 3. Focal mechanisms of type 4 are also normal faults or strike-slip faults. Tensional axes are in the NE-SW direction. These results suggested that extensional stress rather than compressional stress dominates in the transitional zone at intermediate depth.

[28] In the transitional zone, the upper surface of the deep seismic zone changes dip rapidly, un unusual earthquake cluster is found on a near vertical plane within the slab and the extensional stress appears to dominate. On the basis of these facts we propose that there is a slab-cracking zone within the Pacific plate, which possibly will grow into a slab disruption in the future. We call this slab-cracking zone the Tokachi-Oki slab-cracking zone. The extensional stresses are caused by the rapid lateral change in subduction angle, tearing the inside of the slab and forming the near vertical slab-cracking zone within the subducting Pacific slab.

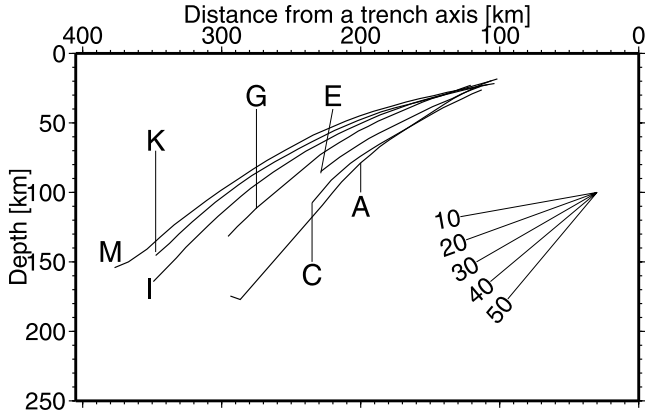

Figure 11. Superposition of the upper surface of the deep seismic zone for profiles A to M. Lines on right show dip angles of 10° to 50°.

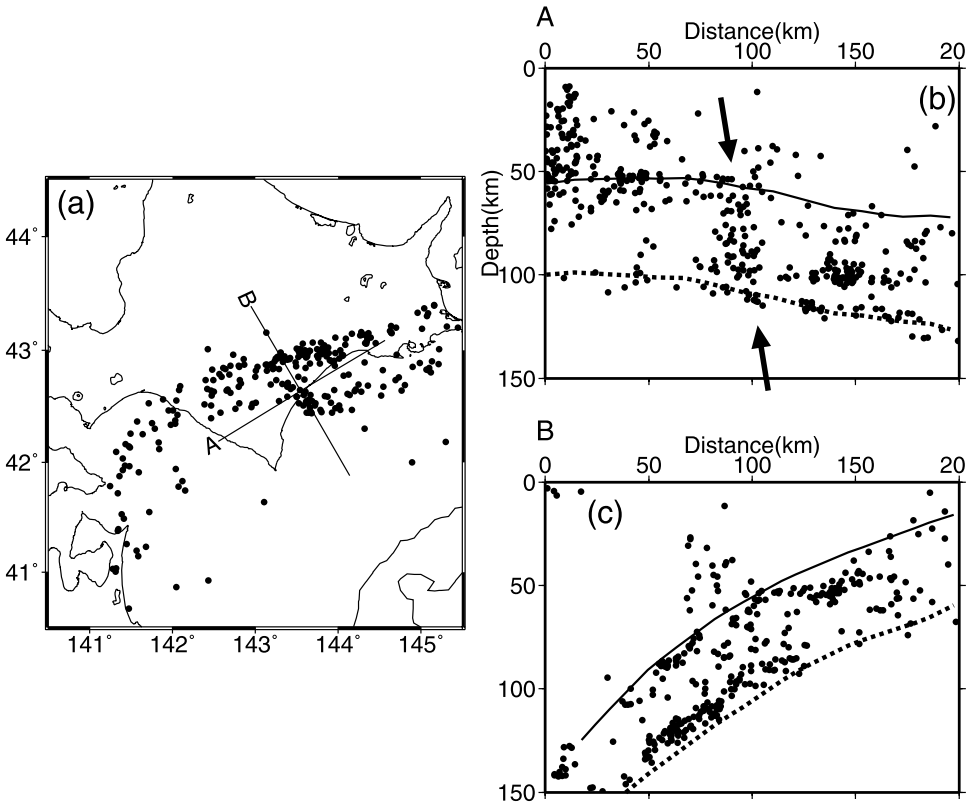

Figure 12. Unusual distribution of earthquakes. (a) Earthquakes located at depths between 80 and 95 km from August 1999 to June 2001. Lines A and B show orientations for cross sections. (b) and (c) Cross sections for lines in Figure 12a with a width of 30 km. The arrows point to the unusual seismicity on a near-vertical plane within the Pacific plate.

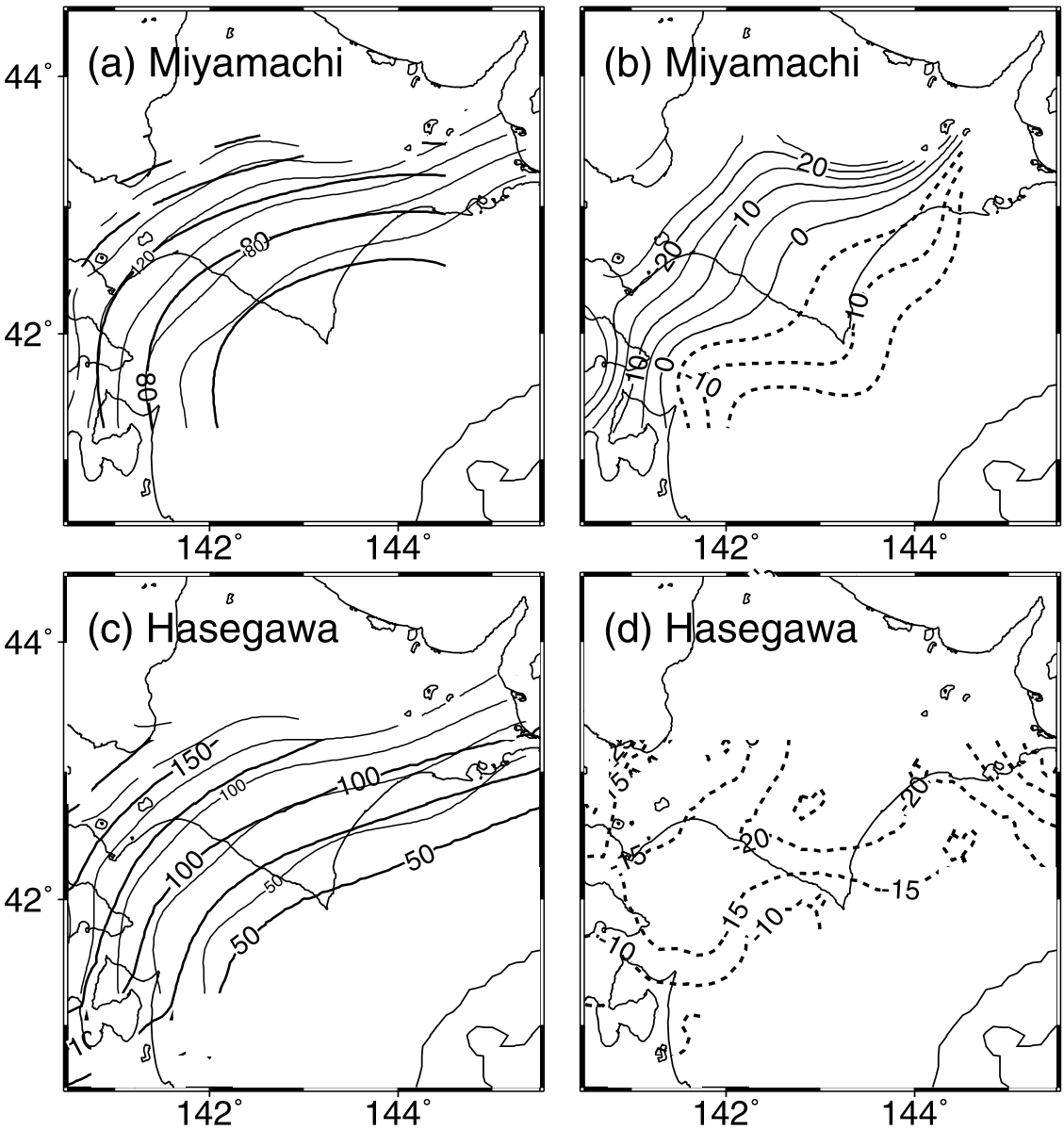

Figure 13. Comparisons of the upper boundary of the Pacific plate determined in this study and previous studies. (a) and (b) Comparisons with *Miyamachi et al.* [1994]. (c) and (d) Comparisons with *Hasegawa et al.* [1983]. Contour lines in Figures 13a–13d are drawn every 20, 5, 25, and 5 km, respectively. Thin lines in Figures 13a and 13c denote the upper boundary determined by the present study. The depth differences $D_{\text{present}} - D_{\text{previous}}$ are shown in Figures 13b and 13d, where D_{present} and D_{previous} are the depths determined by the present and previous studies, respectively. Solid and dashed lines in Figures 13b and 13d denote positive and negative contours, respectively.

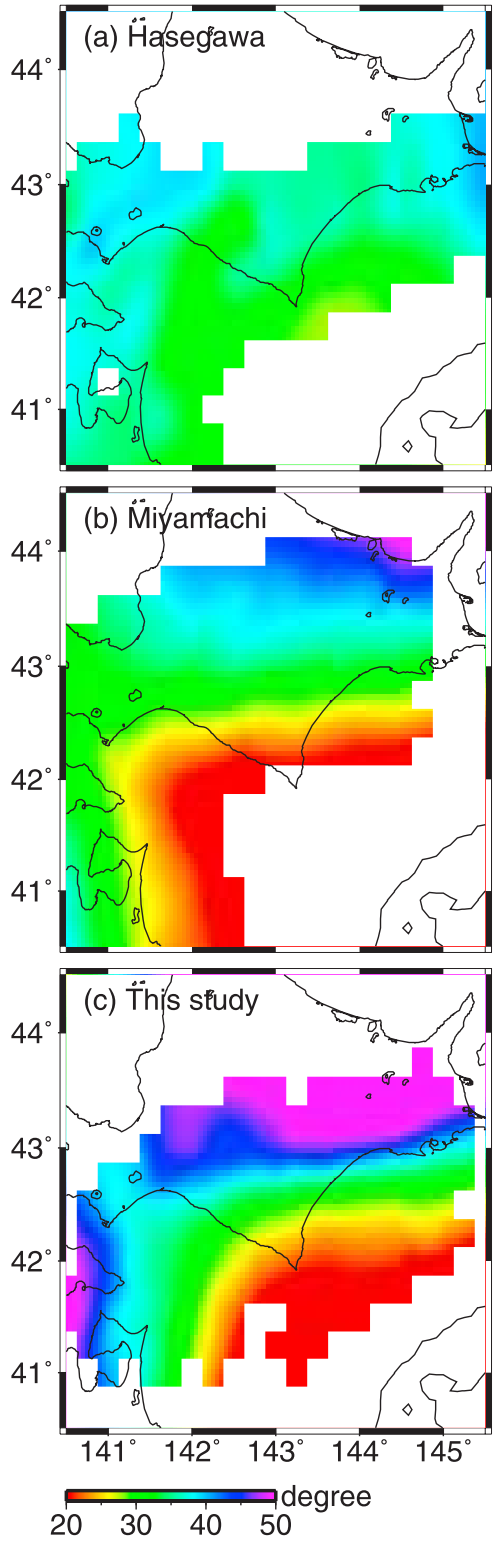

Figure 14. Slope of the upper boundary of the Pacific plate calculated from the models of (a) *Hasegawa et al.* [1983], (b) *Miyamachi et al.* [1994] and (c) the present study. The maximum slope was measured in degrees from the horizontal. Red and violet colors indicate low and high angles, respectively.

6.3. Possibility of Great Lithospheric Earthquake

[29] One of the most important objectives for the mitigation of seismic hazards is to find regions that can potentially have great earthquakes. If the Tokachi-Oki slab-cracking zone found in this study ruptured all at once over its entire area, it would produce a great earthquake. Is this possible? Since there is no established explaining why intermediate-depth earthquakes occur, we are not able to answer to this question. At least we have two clear facts; (1) many small earthquakes with M = 3 or 4 occur within the Tokachi-Oki slab-cracking zone, and (2) great earthquakes have occurred within the Pacific plate in the region from the Hokkaido corner to the southern Kurile Islands; the 1978 M = 7.7 Kunashiri Strait [*Kasahara and Sasatani*, 1985], the 1993 M = 7.8 Kushiro-Oki [*Ide and Takeo*, 1996; *Suzuki and Kasahara*, 1996; *Ozel and Moriya*, 1999] and the 1994 M = 8.2 Hokkaido-Toho-Oki [*Kikuchi and Kanamori*, 1995; *Katsumata et al.*, 1995; *Ozawa*, 1996] earthquakes.

[30] From a statistical point of view, according to the b-value map [*Wiemer and Wyss*, 1997; *Wiemer and Katsumata*, 1999], the b-value in the Tokachi-Oki slab-cracking zone is as low as the neighboring areas within the Pacific plate. The b-value can be perturbed by various reasons. Factors that can result in high b-values include: (1) Increased material heterogeneity or crack density [*Mogi*, 1962], (2) an increase in the thermal gradient [*Warren and Latham*, 1970]. On the other hand, low b-values may be caused by an increase in shear or effective stress [*Scholz*, 1968; *Urbanic et al.*, 1992; *Wyss*, 1973]. The b-value decreases with depth in strike slip fault zones [*Mori and Abercrombie*, 1997; *Wiemer and Wyss*, 1997], is possibly because of the increased applied stress at greater depth. High b-values ($b > 1.3$) are observed in creeping sections of faults [*Amelung and King*, 1997; *Wiemer and Wyss*, 1997], whereas asperities exhibit a low b-value ($b < 0.6$) [*Wiemer and Wyss*, 1997]. The areas of largest slip release during a main shock correlate with high b-value regions in the aftershock zone [*Wiemer and Katsumata*, 1999]. In volcanic areas, high b-values are observed near magma chambers and highly cracked volumes [*Wiemer and McNutt*, 1997; *Wyss et al.*, 1997; *Wiemer et al.*, 1998]. The Tokachi-Oki slab-cracking zone shows low b-value seismicity, which is possibly caused by an increase in shear or effective stress. At least based on the b-value data there is no difference between the areas ruptured by great earthquakes like the 1993 Kushiro-Oki earthquake and the Tokachi-Oki slab-cracking zone.

7. Conclusions

[31] We used a 3-D P and S wave velocity structure, to relocate hypocenters in the region of Hokkaido corner. On the basis of the distribution of the relocated earthquakes we constructed a new model of the geometry of the deep seismic zone in the Pacific plate. The model suggests that the lateral change in dip of the subduction zone is more rapid than previously believed. We found that the deep seismic zone in the Pacific plate dips 20° to 30° on the side of the Japan arc, the dip angle increases in a narrow region around 143–144°E by 10° to 20° and the dip is 40° to 50° on the side of the Kurile arc. In the transitional zone around

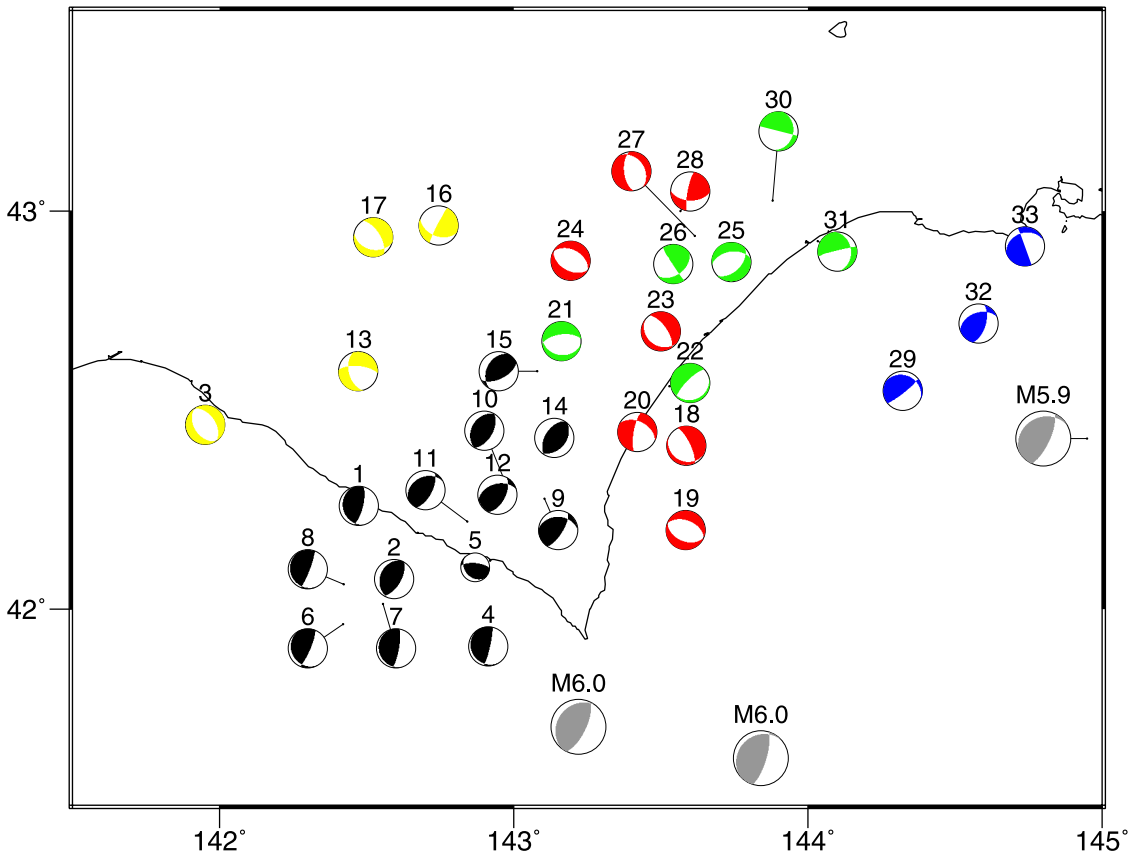

Figure 15. Focal mechanisms on the upper surface of the deep seismic zone determined by plotting first motions of *P* waves. All diagrams are equal area projections of the lower hemisphere of the focal sphere. Numerals in Figure 15 correspond to the event number in Table 2 and in Figure 16. Colored and shaded areas show compressional quadrants. Types 1, 2, 3, 4, and 5 are colored by black, red, green, yellow, and blue, respectively (see text for the types). Focal mechanisms of the events with magnitude 5.9 or larger that occurred between 1990 and 2002 are shown in gray, which were determined by Harvard University.

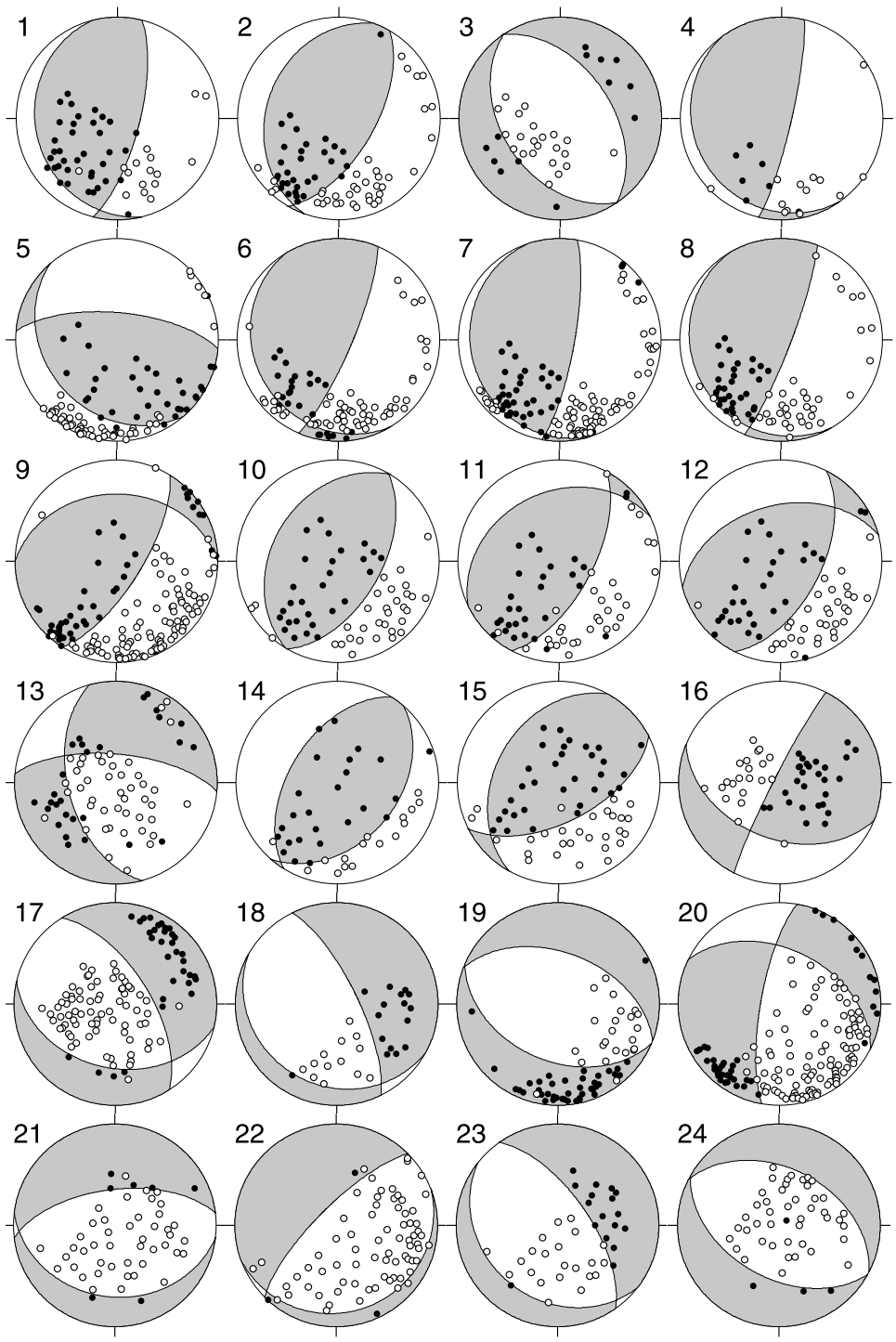

Figure 16. Focal mechanisms on the upper surface of the deep seismic zone determined by plotting first motions of *P* waves. All diagrams are equal area projections of the lower hemisphere of the focal sphere. Numerals in Figure 16 correspond to the event number in Table 2. Solid and open circles indicate compressional and dilatational first motions, respectively. Shaded areas show compressional quadrants.

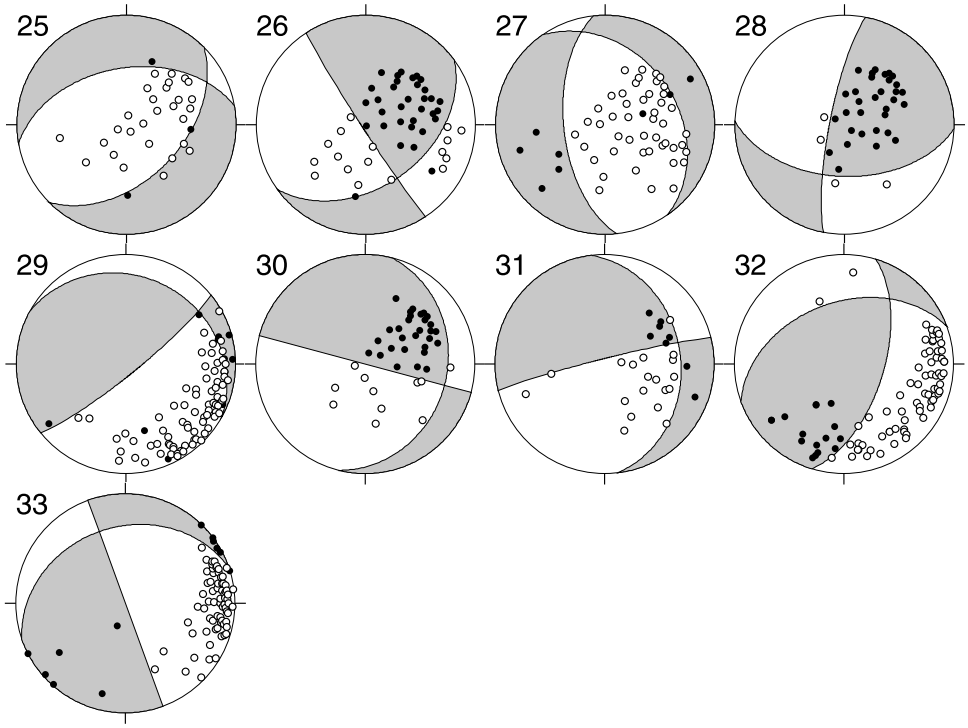

Figure 16. (continued)

Table 2. Hypocentral Data and Fault Plane Solutions[a]

										Fault Plane 1[b]			Fault Plane 2[b]		
Hypocenter	Y	M	D	h	m	Longitude °E	Latitude °N	Depth, km	Magnitude	st	di	sl	st	di	sl
1	2000	02	09	03	24	142.473	42.261	67.3	4.3	14	72	118	166	20	62
2	2000	02	11	11	32	142.593	42.076	56.3	4.9	30	61	100	200	29	80
3	2000	02	26	19	46	141.952	42.465	88.9	3.5	146	42	−90	326	48	−90
4	2000	04	12	12	28	142.913	41.905	39.5	3.0	145	14	42	13	82	138
5	2000	12	02	21	12	142.869	42.106	43.5	4.6	139	29	134	275	68	46
6	2001	03	18	16	18	142.421	41.961	55.2	4.3	149	17	36	23	79	144
7	2001	04	29	01	40	142.556	42.012	58.2	4.9	162	13	62	10	78	118
8	2000	09	03	12	35	142.423	42.063	61.8	4.8	21	82	140	150	12	40
9	2001	05	07	21	27	143.104	42.278	54.1	5.0	32	70	32	270	34	148
10	2000	05	17	20	21	142.975	42.312	54.0	4.3	30	55	89	211	35	91
11	1999	08	15	22	32	142.842	42.221	53.7	4.5	28	63	54	244	32	127
12	2000	10	06	23	19	142.945	42.289	57.2	5.3	27	57	42	255	44	138
13	1999	09	29	00	19	142.471	42.599	83.7	4.2	165	51	−20	275	67	−160
14	2000	11	01	00	20	143.138	42.432	51.3	3.9	41	40	99	212	51	81
15	1999	11	11	20	02	143.081	42.599	73.3	4.1	63	58	124	209	37	56
16	2000	12	17	04	29	142.744	42.965	98.7	3.7	112	44	175	207	85	5
17	2001	05	09	23	05	142.523	42.935	112.3	4.0	103	37	−135	328	62	−45
18	2000	11	04	21	10	143.586	42.413	51.2	3.2	119	20	−126	334	73	−54
19	2000	12	12	21	02	143.584	42.199	48.9	4.2	113	43	−88	291	48	−92
20	2001	04	23	00	04	143.420	42.447	51.4	4.9	296	45	−163	190	75	−17
21	2000	07	06	16	28	143.163	42.675	77.5	3.7	263	61	−104	97	30	−76
22	2000	05	21	14	19	143.528	42.562	53.7	4.9	70	15	−65	225	75	−115
23	2000	09	16	15	41	143.535	42.680	65.8	3.4	325	65	−73	128	27	−107
24	2000	07	03	10	50	143.193	42.877	88.5	3.3	119	47	−88	297	43	−92
25	2000	05	17	08	17	143.739	42.874	76.0	3.3	45	48	−125	260	47	−55
26	1999	12	07	08	33	143.543	42.868	74.0	4.2	54	43	177	147	87	3
27	2000	06	11	10	18	143.616	42.938	81.3	4.0	325	34	−119	174	59	−62
28	2000	07	22	12	27	143.567	43.001	92.2	3.4	191	79	9	92	51	171
29	2001	05	22	05	45	144.323	42.550	47.7	4.5	299	21	158	51	82	22
30	2000	09	18	14	59	143.880	43.026	85.3	3.5	105	90	1	14	26	179
31	2001	03	02	02	21	144.033	42.926	77.5	3.4	256	86	−7	353	31	−173
32	2000	11	15	14	19	144.580	42.719	58.4	5.2	17	60	37	250	43	143
33	2000	06	12	16	54	144.737	42.912	65.2	5.7	160	90	−1	251	31	−179

[a]Origin times are in UT.
[b]Abbreviations st, di, and sl stand for strike, dip, and slip in degree in Harvard convention, respectively. Abbreviations Y, M, D, h, and m stand for year, month, day, hour, and minute.

143–144°E an unusual distribution of microearthquakes has been discovered within the Pacific plate, which was located on a near-vertical plane with an area of 50 × 100 km^2 and strike perpendicular to the Kurile Trench axis. This feature was named the Tokachi-Oki slab-cracking zone. We suggest that the Tokachi-Oki slab-cracking zone is in the initial stage of slab tearing. From a point of seismic hazards, if the Tokachi-Oki slab-cracking zone found in this study ruptured all at once over its entire area, it would produce a great earthquake.

[32] **Acknowledgments.** We thank Dapeng Zhao at Ehime University for providing computer software for the 3-D hypocenter determination. The comments from two reviewers, Jeff Park and Matthew Fouch, and the Associate Editor were very helpful in revising the manuscript. We also thank James Mori at Kyoto University for polishing the language in the manuscript. We used waveform data from seismic stations maintained by Hokkaido University, Hirosaki University, Tohoku University, Sapporo City, JMA and NIED. This research is supported by the "New Program for Earthquake Prediction Research and Observations" in Japan [*Hirata*, 2000]. GMT [*Wessel and Smith*, 1991] was used to make figures.

References

Abe, K., Tsunami and mechanism of great earthquake, *Phys. Earth Planet. Inter.*, *7*, 143–153, 1973.

Amelung, F., and G. King, Earthquake scaling laws for creeping and non-creeping faults, *Geophys. Res. Lett.*, *24*, 507–510, 1997.

Burbach, G. V., and C. Frohlich, Intermediate and deep seismicity and lateral structure of subducted lithosphere in the circum-Pacific region, *Rev. Geophys.*, *24*, 833–874, 1986.

Chiu, J., B. L. Isacks, and R. K. Cardwell, 3-D configuration of subducted lithosphere in the western Pacific, *Geophys. J. Int.*, *106*, 99–111, 1991.

DeMets, C., Oblique convergence and deformation along the Kuril and Japan trenches, *J. Geophys. Res.*, *97*, 17,615–17,625, 1992.

DeMets, C., R. G. Gordon, D. F. Argus, and S. Stein, Effect of recent revisions to the geomagnetic reversal time scale on estimates of current plate motions, *Geophys. Res. Lett.*, *21*, 2191–2194, 1994.

Fukao, Y., and M. Furumoto, Stress drops, wave spectra and recurrence intervals of great earthquakes—Implications of the Etorofu earthquake of 1958 November 6, *Geophys. J. R. Astron. Soc.*, *57*, 23–40, 1979.

Hasegawa, A., N. Umino, and A. Takagi, Double-planed structure of the deep seismic zone in the northeastern Japan arc, *Tectonophysics*, *47*, 43–58, 1978.

Hasegawa, A., N. Umino, A. Takagi, S. Suzuki, Y. Motoya, S. Kameya, K. Tanaka, and Y. Sawada, Spatial distribution of earthquakes beneath Hokkaido and Northern Honshu, Japan (in Japanese), *J. Seismol. Soc. Jpn.*, *36*, 129–150, 1983.

Hashimoto, M., Finite element modeling of deformations of the lithosphere at an arc-arc junction: The Hokkaido corner, Japan, *J. Phys. Earth*, *32*, 373–398, 1984.

Hirata, N., Promotion of new programs on study and observation for earthquake forecast, paper presented at Third Joint Meeting, Panel on Earthquake Res., The U.S.-Jpn. Coop. Program in Nat. Resour., Menlo Park, Calif., 13–15 Nov., 2000.

Hirata, N., and M. Matsu'ura, Maximum-likelihood estimation of hypocenter with origin time eliminated using nonlinear inversion technique, *Phys. Earth Planet. Inter.*, *47*, 50–61, 1987.

Ide, S., and M. Takeo, The dynamic rupture process of the 1993 Kushiro-oki earthquake, *J. Geophys. Res.*, *101*, 5661–5675, 1996.

Isacks, B., and P. Molnar, Distribution of stresses in the descending lithosphere from a global survey of focal mechanism solutions of mantle earthquakes, *Rev. Geophys.*, *9*, 103–174, 1971.

Kanamori, H., Focal mechanism of the Tokachi-Oki earthquake of May 16, 1968: Contortion of the lithosphere at a junction of two trenches, *Tectonophysics*, *12*, 1–13, 1971.

Kasahara, M., Vertical crustal movement around Cape Erimo, southern part of Hokkaido and a brief of the recent crustal movement of Hokkaido region (in Japanese), paper presented at Symposium on Subterranean Structure in and Around Hokkaido and its Tectonic Implication, Inst. of Seismol. and Volcanol., Hokkaido Univ., Sapporo, Japan, 1976.

Kasahara, M., and T. Sasatani, Source characteristics of the Kunashiri strait earthquake of December 6, 1978 as deduced from strain seismograms, *Phys. Earth Planet. Inter.*, *37*, 124–134, 1985.

Katsumata, K., M. Ichiyanagi, M. Miwa, M. Kasahara, and H. Miyamachi, Aftershock distribution of the October 4, 1994 *Mw*8.3 Kurile Islands earthquake determined by a local seismic network in Hokkaido, Japan, *Geophys. Res. Lett.*, *22*, 1321–1324, 1995.

Katsumata, K., et al., Distribution of hypocenters and focal mechanisms in and around the Hidaka arc-arc collision zone revealed by a dense temporary seismic network (in Japanese), *Bull. Earthquake Res. Inst. Univ. Tokyo*, *77*, 199–223, 2002a.

Katsumata, K., N. Wada, and M. Kasahara, Three-dimensional *P* and *S* wave velocity structures beneath the Hokkaido corner, Japan-Kurile arc-arc junction, paper presented at Fall Meeting of the Seismological Society of Japan, Seismol. Soc. of Jpn., Yokohama, Japan, 2002b.

Kikuchi, M., and H. Kanamori, The Shikotan earthquake of October 4, 1994: Lithospheric earthquake, *Geophys. Res. Lett.*, *22*, 1025–1028, 1995.

Kimura, G., Collision orogeny at arc-arc junctions in the Japanese Islands, *Isl. Arc*, *5*, 262–275, 1996.

Kosuga, M., T. Sato, A. Hasegawa, T. Matsuzawa, S. Suzuki, and Y. Motoya, Spatial distribution of intermediate-depth earthquakes with horizontal or vertical nodal planes beneath northeastern Japan, *Phys. Earth Planet. Inter.*, *93*, 63–89, 1996.

Lundgren, P., and D. Giardini, Lateral structure of the subducting Pacific plate beneath the Hokkaido corner from intermediate and deep earthquakes, *Pure Appl. Geophys.*, *134*, 385–404, 1990.

Miyamachi, H., M. Kasahara, S. Suzuki, K. Tanaka, and A. Hasegawa, Seismic velocity structure in the crust and upper mantle beneath northern Japan, *J. Phys. Earth*, *42*, 269–301, 1994.

Mogi, K., Magnitude-frequency relation for elastic shocks accompanying fractures of various materials and some related problems in earthquakes, *Bull. Earthquake Res. Inst. Univ. Tokyo*, *40*, 831–853, 1962.

Mori, J., and R. E. Abercrombie, Depth dependence of earthquake frequency-magnitude distributions in California: Implications for rupture initiation, *J. Geophys. Res.*, *102*, 15,081–15,090, 1997.

Moriya, T., Seismic studies of the upper mantle beneath the arc-junction at Hokkaido: Folded structure of intermediate-depth seismic zone and attenuation of seismic wave, *J. Phys. Earth*, *26*, suppl., S467–S475, 1978.

Moriya, T., H. Okada, T. Matsushima, S. Asano, T. Yoshii, and A. Ikami, Collision structure in the upper crust beneath the southwestern foot of the Hidaka Mountains, Hokkaido, Japan as derived from explosion seismic observations, *Tectonophysics*, *290*, 181–196, 1998.

Ozawa, S., Geodetic inversion for the fault model of the 1994 Shikotan earthquake, *Geophys. Res. Lett.*, *23*, 2009–2012, 1996.

Ozel, N., and T. Moriya, Different stress directions in the aftershock focal mechanisms of the Kushiro-Oki earthquake of Jan. 15, 1993, SE Hokkaido, Japan, and horizontal rupture in the double seismic zone, *Tectonophysics*, *313*, 307–327, 1999.

Sasatani, T., Mechanism of mantle earthquakes near the junction of the Kurile and the northern Honshu arcs, *J. Phys. Earth*, *24*, 341–354, 1976.

Scholz, C. H., The frequency-magnitude relation of microfracturing in rock and its relation to earthquakes, *Bull. Seismol. Soc. Am.*, *58*, 399–415, 1968.

Stauder, W., and L. Mualchin, Fault motion in the larger earthquakes of the Kurile-Kamchatka arc and of the Kurile-Hokkaido corner, *J. Geophys. Res.*, *81*, 297–308, 1976.

Suzuki, S., and M. Kasahara, Unbending and horizontal fracture of the subducting Pacific plate, as evidenced by the 1993 Kushiro-oki and the 1981 and 1987 intermediate-depth earthquakes in Hokkaido, *Phys. Earth Planet. Inter.*, *93*, 91–104, 1996.

Suzuki, S., T. Sasatani, and Y. Motoya, Double seismic zone beneath the middle of Hokkaido, Japan, in the southwestern side of the Kurile arc, *Tectonophysics*, *96*, 59–76, 1983.

Suzuki, S., T. Takanami, Y. Motoya, and I. Nakanishi, A real-time automatic processing system of seismic waves for the network of Hokkaido Univ. (in Japanese), *J. Seismol. Soc. Jpn.*, *41*, 359–373, 1988.

Takahashi, H., et al., Velocity field of around the Sea of Okhotsk and Sea of Japan regions determined from a new continuous GPS network data, *Geophys. Res. Lett.*, *26*, 2533–2536, 1999.

Tsumura, N., H. Ikawa, T. Ikawa, M. Shinohara, T. Ito, K. Arita, T. Moriya, G. Kimura, and T. Ikawa, Delamination-wedge structure beneath the Hidaka Collision Zone, central Hokkaido, Japan inferred from seismic reflection profiling, *Geophys. Res. Lett.*, *26*, 1057–1060, 1999.

Urbanic, T. I., C. I. Trifu, J. M. Long, and R. P. Toung, Space-time correlations of *b* values with stress release, *Pure Appl. Geophys.*, *139*, 449–462, 1992.

Utsu, T., Distribution of earthquake hypocenters in and around Japan (in Japanese), *Kagaku Tokyo*, *44*, 739–746, 1974.

Warren, N. W., and G. V. Latham, An experimental study of thermally induced microfracturing and its relation to volcanic seismicity, *J. Geophys. Res.*, *75*, 4455–4464, 1970.

Wessel, P., and W. H. F. Smith, Free software helps map and display data, *Eos Trans. AGU*, *72*, 441, 445–446, 1991.

Wiemer, S., and K. Katsumata, Spatial variability of seismicity parameters in aftershock zones, *J. Geophys. Res.*, *104*, 13,135–13,151, 1999.

Wiemer, S., and S. McNutt, Variations in the frequency-magnitude distribution with depth in two volcanic areas: Mount St. Helens, Washington, and Mt. Spurr, Alaska, *Geophys. Res. Lett.*, *24*, 189–192, 1997.

Wiemer, S., and M. Wyss, Mapping the frequency-magnitude distribution in asperities: An improved technique to calculate recurrence times?, *J. Geophys. Res.*, *102*, 15,115–15,128, 1997.

Wiemer, S., S. R. McNutt, and M. Wyss, Temporal and three-dimensional spatial analysis of the frequency-magnitude distribution near Long Valley Caldera, California, *Geophys. J. Int.*, *134*, 409–421, 1998.

Wyss, M., Towards a physical understanding of the earthquake frequency distribution, *Geophys. J. R. Astron. Soc.*, *31*, 341–359, 1973.

Wyss, M., K. Shimazaki, and S. Wiemer, Mapping active magma chambers by *b* values beneath the off-Ito volcano, Japan, *J. Geophys. Res.*, *102*, 20,413–20,433, 1997.

Zhao, D., A. Hasegawa, and S. Horiuchi, Tomographic imaging of *P* and *S* wave velocity structure beneath northeastern Japan, *J. Geophys. Res.*, *97*, 19,909–19,928, 1992.

M. Kasahara and K. Katsumata, Institute of Seismology and Volcanology, Hokkaido University, North-10, West-8 Sapporo 060-0810, Japan. (mkasa@eos.hokudai.ac.jp; katsu@eos.hokudai.ac.jp)

N. Wada, Shibetsu-cho Town Office, Shibetsu-cho, Japan. (wada_naoto@shibetsutown.jp)